



School of Chemistry

**Boron Doped Diamond Nanoparticles As
Seeds For Non-Diamond Substrates**

Miran Tsang

This thesis is submitted in partial fulfilment of the requirements for the Honours degree
of MSci at the University of Bristol

Supervisor: Dr Neil Fox

Second Assessor: Professor Paul May

Abstract

Boron doped diamond (BDD) was used as seeds for non-diamond substrates to create a conductive layer that reduces resistance at the diamond-substrate interface. A top-down, bottom up method has been reported, where a microcrystalline BDD (made from using the chemical vapour deposition (CVD) technique) was bead milled into nanoparticles (top-down approach) and used as seeds for subsequent CVD regrowth.

After optimisation and analysis, the best seeding method was identified. A combination of cationic polymer poly(ethylenimine) PEI and BDD suspension in an alkaline buffer was used to seed the substrates and a nucleation density $6.70 \times 10^8 \text{ cm}^{-2}$ was achieved. Dynamic light scattering (DLS) and scanning electron microscopy (SEM) calculated results show a large particle size distribution of the pulverised particles in suspension form and on the substrate surface. The distributions were $\sim 150\text{-}650$ nm and $50\text{-}700$ nm respectively. The seeded substrates were regrown (bottom-up approach) in a hot filament CVD reactor (HFCVD) using different boron concentrations and growth times; results were compared with substrates seeded with undoped detonation nanodiamond (DND).

The surface morphology of BDD grown on doped seeds was relatively inhomogeneous and mainly consisted of twinned (111) material; a continuous film was observed at 30 minutes growth. BDD grown on undoped seeds had smaller grain sizes ($\sim 100\text{-}500$ nm) due to smaller parent seeds that were equal in size.

Resistance results show the BDD grown on doped seeds with PEI were relatively resistant in comparison with BDD grown on undoped seeds and doped seeds without PEI. This may be due to the absorbed polymer layer acting as a resistive barrier, or the PEI (nitrogen containing species) acting as a mediator in the enhancement of undoped growth during CVD stages. The interfacial resistance was only marginally different between doped seeds without PEI and undoped seeded substrates ($\sim 20\text{-}40 \Omega$); thus improvement in interfacial conductivity with doped seeds was not observed. This may be due to incomplete oxygen termination of the diamond surface or the large variation of particle sizes found in doped seeds which could disrupt conduction pathways.

Table of Contents

Abstract	1
Acknowledgements	4
1. Introduction	5
1.1. General Properties of Diamond	5
1.2. Intrinsic Semiconductors	7
1.3. Extrinsic Semiconductor - Doping	7
1.3.1. Band Bending	10
1.4. Diamond Synthesis	11
1.4.1. Chemical Vapour Deposition (CVD) of Diamond	12
1.5. Nucleation Techniques	15
1.5.1. Seeding Methods	16
1.6. Boron Doped Nanoparticles	17
2. The Diamond-Substrate Interface	19
2.1. Particle Size Separation	19
2.2. Acid Treatment for Impurity Removal and Oxidative Removal of sp^2 Carbon	19
2.3. Preparing a Stable Diamond Suspension	20
2.3.1. Surface Modification of Boron Doped Diamond	22
2.3.2. Surface Modification of Substrate	22
2.3.3. The Choice of Substrate	23
2.4. Mechanical and Chemical De-agglomeration	24
2.5. The CVD Diamond Film	25
2.6. Project Aims	25
2.7. Applications	26
2.7.1. Diamond Electrodes	26
2.7.2. Low Melting Point Substrates	26
2.7.3. Surface Termination and Electron Affinity	27
3. Experimental	29
3.1. Materials	29
3.2. Preparation	29
3.2.1. Bead Milling	29
3.2.2. Acid Treatment	29
3.2.3. Sample Fabrication – Seeding Methods	30
3.2.4. CVD Diamond Growth	33

3.3.	Characterisation.....	34
3.3.1.	Dynamic Light Scattering (DLS).....	34
3.3.2.	Zeta Potential.....	34
3.3.3.	Scanning Electron Microscopy (SEM).....	35
3.3.4.	Resistance Test for Electrical Conductivity.....	36
4.	Results and Discussion.....	37
4.1.	pH Studies.....	37
4.2.	DLS Measurements.....	37
4.3.	Zeta Potential Measurements.....	38
4.4.	SEM Results.....	40
4.5.	Resistance Measurements.....	46
5.	Conclusion.....	48
6.	Future Work.....	50
6.1.	Method Development.....	50
6.1.1.	DLS - Method Development.....	50
6.1.2.	Zeta Potential Measurements – Method Development.....	50
6.1.3.	Resistance Measurements - Method Development.....	50
6.2.	Further Suggestions.....	51

List of Acronyms

AFM = Atomic Force Microscopy
BDD = Boron Doped Diamond
CVD = Chemical Vapour Deposition
DLS = Dynamic Light Scattering
DND = Detonation Nanodiamond
HET = Heterogeneous Electron Transfer
NEA = Negative Electron Affinity
PDDA = Poly(diallyldimethylammonium chloride)
PEA = Positive Electron Affinity
PEI = Poly(ethylenimine)
PSS = Poly(sodium 4-styrenesulfonate)
SEM = Scanning Electron Microscopy
SIMS = Scanning Ion Mass Spectrometry
SSRM = Scanning Spreading Resistance Microscopy
STM = Scanning Tunnelling Microscopy

Acknowledgements

Special thanks to Dr. Neil Fox and Professor Paul May for their advice and guidance throughout my project. I would especially like to thank Dr. Zamir Othman for working with me on this project and offering me invaluable support.

I would like to thank Alex, Sarah, and Hugo for training me on various instruments and giving me plenty of advice on a day-to-day basis. Thanks to James for fixing the lab machinery and Ben, Cathy and Jan for helping me out in the lab. Thanks to Jamie for proof reading my work and practicing my presentation with me. I would also like to thank Hannah for offering me lots of assistance in the lab and being a brilliant laugh in and outside of university.

Final thanks to the BUDGies, the BTDC group and everyone else involved in the project for their support and the interest shown in my work.

1. Introduction

1.1. General Properties of Diamond

There has been a growing interest in studying the physical properties of diamond and its range of applications have long since expanded from the mere aesthetics of diamond gemstones.¹ Some of the properties are outlined in Table 1.

Table 1. General properties of diamond²

Mechanical Hardness	90 GPa
Bulk Modulus	$1.2 \times 10^{12} \text{ Nm}^{-2}$
Compressibility	$8.3 \times 10^{-13} \text{ m}^2 \text{ N}^{-1}$
Thermal Conductivity	$2 \times 10^3 \text{ W m}^{-1} \text{ K}^{-1}$
Thermal Expansion Coefficient (25° C)	$1.1 \times 10^{-6} \text{ K}$
Band Gap	5.45 eV
Resistivity (25° C)	$10^{16} \Omega \text{ cm}$
Electron Mobility	$2200 \text{ cm}^2 \text{ V}^{-1} \text{ s}^{-1}$
Carrier Mobility (Electron and Hole)	$3800 \text{ cm}^2 \text{ V}^{-1} \text{ s}^{-1}$
Young's Modulus	1.22 GPa
Refractive Index	2.42
Density	3.52 g cm^{-3}

Diamond has the highest mechanical hardness and thermal conductivity at room temperature of any material. It is also the least compressible material and is chemically inert to most reagents. These desirable properties are employed for cutting, polishing, drilling, and engineering applications.³

These properties are not easily accessible due to the fact that diamond is not the most thermodynamically stable allotrope of carbon and under standard conditions, graphite will usually be synthesised due to its relatively low energy barrier. However, diamond is considered to be metastable, meaning it is kinetically stable rather than thermodynamically stable; once the large activation barrier between graphite and diamond is overcome ($728 \pm 50 \text{ kJ mol}^{-1}$), the two will not spontaneously interconvert via thermal activation despite their standard enthalpies being only 2.9 kJ mol^{-1} apart.⁴

As mentioned, the two most common allotropes of carbon are graphite and diamond. Graphite is made of layered sheets of sp^2 bonded carbons that form hexagonal ring structures and each carbon gives one delocalised electron in the system. On the other hand, the diamond structure contains no delocalised

electrons as all the carbons are sp^3 bonded to the neighbouring carbon atoms to form a tetrahedral lattice. The two structures are shown on Figure 1.

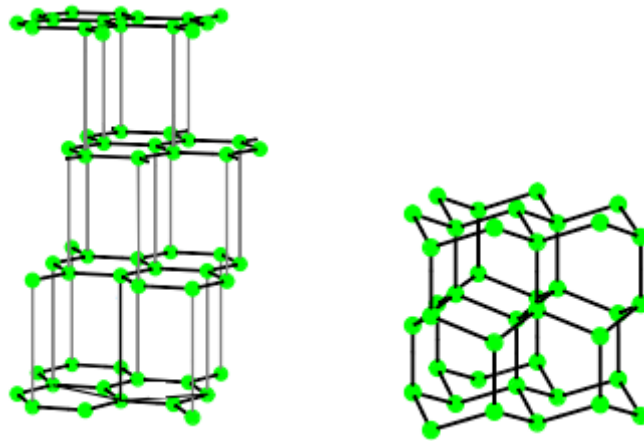


Figure 1. Allotropes of carbon: graphite (left) and diamond (right)⁵

In the simple harmonic model, the vibrational motion of a molecule is depicted as the oscillation of a spring. The frequency of this motion is proportional to the restoring force and is inversely proportional to the displacement from its equilibrium position (which in turn is affected by the mass of the vibrating atoms). This relation explains why diamond has such high thermal conductivity, for the carbon atoms are light and the covalent bonds between them are strong (347 kJ mol^{-1}). Diamond has very high vibrational frequencies exceeding many metals, for example its thermal conductivity is four times larger than copper at room temperature⁶.

The band gap of a material is the energy difference between the valence band maximum and the conduction band minimum in an electronic band structure. Large band gap materials are considered to be insulators whereas small band gap materials are either conducting or semi-conducting. For each material, a minimum energy is required to move the outer shell electron in between bands, and this is gained from either absorbing a phonon (heat) or photon (light). The band gap can also be decreased when temperature is increased.

Diamond has a band gap of 5.45 eV and is considered a wide and indirect band gap material. Indirect band gap means the momentum of electrons is not the same in both valence and conduction bands hence a photon can only be emitted via an intermediate phonon assisted transition state. Although it is highly insulating in its pure form, its semiconducting and conducting properties can be activated via

doping (see section 1.2) Wide band gap materials are more voltage tolerant which makes it a more powerful semi-conductor material compared with Si (1.1 eV) and Ge (0.7 eV) analogues.

Diamond is chemically stable to oxygen and does not support a native oxide like Ge and Si. Diamond is naturally an electrical insulator and in the absence of an oxide layer, the surface can be functionalised with other elements and compounds to alter its surface properties, and this opens up the possibility of many other useful applications which are explained later.

1.2. Intrinsic Semiconductors

Intrinsic semiconductors are small band gap materials with full valence and empty conduction bands. The electrons from the valence band can be excited by heat or light and travel across the band gap to the conduction band. This results in two partially filled bands and the electrons within the band become mobile and allow current flow. Electronic conductivity of intrinsic semiconductors depends on the number of charge carriers which increases with temperature increase.

There are two types of intrinsic defects. Schottky defects simultaneously generate cation and anion vacancies in the lattice in order to maintain electronic neutrality. Frenkel defects involve ions moving from the normal lattice into interstitial positions which are not normally occupied by lattice atoms; the number of vacant sites is equal the number of interstitial atoms.

The generated vacancies allow enhanced mobility of ions and hence the number of current carriers increases with increase in defects.

1.3. Extrinsic Semiconductor - Doping

Doping is a method of implementing trace impurities or dopant atoms in the crystal lattice of the base material. In an undoped semiconductor such as silicon, there are electrons which can move across the band gap from the valence to the conduction band. This creates a “hole” in the regular Si lattice, and under the influence of an external voltage, both the electron and the “hole” can move across the bulk. But the conductivity of undoped semiconductors is highly dependent on temperature and the number of defects found naturally within the crystal. When introducing even the smallest amount of impurities into the system, the conductivity can be enhanced at low temperatures by many orders of magnitude⁷.

Dopant atoms can situate on a site that is usually occupied by the semiconductor atom, i.e. in the substitutional position in the lattice. These atoms are usually larger than the lattice atoms and thus cannot fit in other sites. In the case of smaller atoms (less than 60% the radius of the parent atom), the

dopant atoms can also occupy interstitial positions in the lattice which are not usually occupied by the semiconductor atoms. This involves atoms jumping from one interstitial position to another.⁸

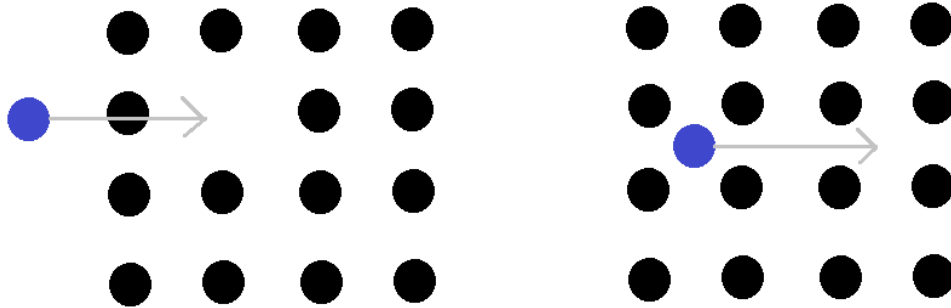


Figure 2. Illustration of substitutional doping (left) and interstitial doping (right); the blue spot represents the dopant atom and the black spots represent the atoms within the lattice

Diamond is an extrinsic semiconductor where intentional doping is used to alter the electronic properties of the material. Many dopants are unsuitable for replacing the carbon atoms due to the small tetrahedral radius of carbon in the diamond lattice structure (interatomic radius 0.77 \AA) and this leads to distortions of the unit cell which is highly energetically unstable. Most natural diamonds contain intrinsic Frenkel defects where N atoms are found to be located on interstitial sites. However in synthetic diamond, extrinsic nitrogen and boron impurities have shown to be substitutional.⁹

Boron is generally thought of as the best candidate dopant due to its similarity in size with carbon but nitrogen and phosphorus along with a few others are also known dopant materials¹⁰. These atoms generate electronic states between the band gap and change the bulk electronic structure of diamond, which in turn influences the current flow in the semiconductor. The number of charge carriers depends on the dopant energy levels and is also temperature dependent. However, the charges are weakly bound to the atoms and current can flow relatively easily. Hence electrical conductivity greatly increases even at low dopant levels and at ambient temperatures.

The electronegativity of the elemental impurity also influences the choice of dopants. In a binding situation, the more electronegative species bind the electrons more strongly thus carry a net negative charge. In the case where there is a surplus of electrons from an n-type dopant, the electrons are weakly bound and can easily escape into the conduction band; these types of impurities are known as donors. Oppositely, a more electropositive dopant would be an acceptor and electrons from the valence band can easily escape into the impurity band (Figure 3).

Boron produces p-type conductivity when introduced into the diamond lattice as a substitutional elemental impurity. This energy level acts as an acceptor/ positive hole and it sits near the top of the valence band about 0.37 eV apart¹¹. As the boron concentration increases, the acceptor energy levels broaden. These energy levels interact with the top valence band and eventually lead to a continuum of energies at the Fermi level; hence electronic conductivity is accomplished (Figure 4). Alternatively, the electrons in the valence band can be thermally excited into the empty acceptor levels at minimal excitation energy.

Boron doped diamond (BDD) has a wide potential window, low double layer capacitance, chemical inertness and structural stability¹²; these properties are desirable in the electrode industry (section 2.7.1.)

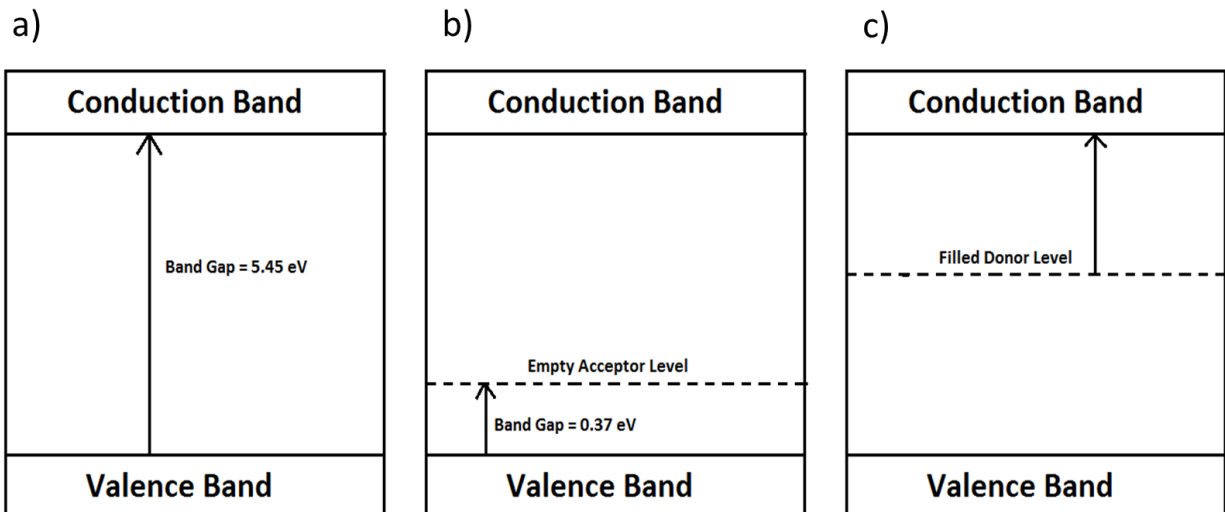


Figure 3. Schematic showing the band gaps of a) Undoped diamond, b) p-doped diamond where electron deficient atoms generate empty acceptor levels above the valence band (value stated refers to boron-doped diamond) and c) n-doped diamond (generic) where a surplus of electrons generate filled donor levels below the conduction band

N-type doping is achieved by the more electronegative elements such as nitrogen and phosphorus and is the opposite to p-type dopants. With more electrons than carbon, n-type dopants substitute carbon atoms and the energy levels act as a donor / surplus of electron density near the conduction band minimum. N-type doping is less easily achieved for there are few elements of similar covalent radius which are able to occupy the vacant site of carbon. Furthermore the gap between the donor level and the conduction band minimum is much greater than that of the acceptor level and the valence band maximum in the nitrogen case (~ 1.7 eV)¹³. Hence despite having the ability to displace carbon atoms,

nitrogen is not able to provide sufficient conductivity at room temperature due to its deep donor energy levels.¹⁴

However, when the donor level is situated near the conduction band minimum, the work function Φ is greatly reduced. This allows the diamond to become an electron source in a vacuum, which consequently emits electrons from the bulk to the surface via excitation methods at a much lower activation barrier than the undoped equivalent. These advantages could find its uses in the electron emission industry thus methods of efficient, successful n-type doping is still of high interest¹⁵.

1.3.1. Band Bending

The Fermi level is the energy gap separating the occupied valence states from the empty conduction states. For intrinsic semiconductors, the Fermi level is exactly in the middle of the energy band gap, and all the energy levels below the Fermi level are filled with electrons. This is only a theoretical statement as there are no energy states in the band gap for a purely intrinsic semiconductor; the Fermi level is simply the probability of the energy states being filled if the states had existed.

In terms of Fermi-Dirac quantum statistics, the distribution of energy states are made up of electrons and holes; the particles are known as “Fermion” particles which have half-integer spin. These particles obey the Pauli Exclusion Principle, which states that no two particles can occupy identical quantum numbers. Additionally, the particles obey the mass action law (Equation 1) which states the product of free electron e^- and hole carrier h^+ concentration is equal to the square of the intrinsic carrier concentration n_i :

$$[e^-][h^+] = n_i^2$$

Equation 1. Equation of the law of mass action

In an extrinsic semiconductor, the two conditions still hold and electronic neutrality must be conserved. This infers that the Fermi level must move away from the middle position. For a p-type semiconductor, the Fermi level shifts towards the top valence band where the number of donors is lower than the number of acceptors; the change in band structure is said to be downward band bending. Oppositely, an n-type semiconductor shifts the Fermi level towards the conduction band where the number of donors is higher the number of acceptors, thus causing upward band bending.

As the p-type dopant is introduced, the empty acceptor levels become filled as electrons from the valence band are promoted. As mentioned, conduction occurs through electronic means as the number

of charge carriers increase. However, another conduction mechanism can take place at high impurity levels. As the dopant concentration increases, the number of filled impurity energy states increase and eventually broadens into an impurity band. This band can now undergo charge hopping conduction through nearest neighbours and the bulk structure can be changed.

At high enough dopant concentration, the impurity band could in theory merge with the valence band and the energy states can mix, thereby inducing metallic-like conductivity (Figure 4). Interestingly, a drop in charge mobility can sometimes be observed at such levels and it has been suggested that this is due to the enhancement of grain boundary effects. It is predicted the non-diamond impurities have a tendency of accumulating at the grain boundaries, causing increased scattering of the current carriers thus a slight decrease in conductivity.¹⁶

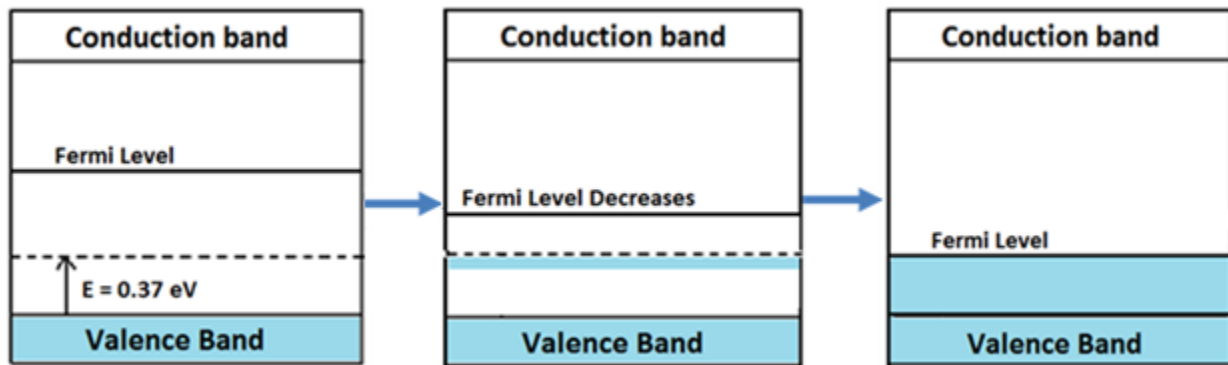


Figure 4. Schematic demonstrating the effects of dopant concentration on conductivity. The parts shaded blue indicate filled energy levels and the direction of the blue arrows indicate the increase in dopant concentration

It has been reported by Takano et al. the synthesis of superconductive, highly boron-doped diamond can be achieved at high pressure (100,000 atm) and high temperature (2500-2800 K). Boron doped diamond is found to be a bulk type II superconductor below critical temperature $T_c \approx 4$ K and the upper critical field H_{c2} is ≥ 3.5 T at 0 K which is the magnetic field at which superconductivity is completely suppressed.¹⁷ It is also possible to achieve superconductivity via chemical vapour deposition. The onset for zero resistance is $T_c \approx 4.2$ K with the onset of superconducting transition 7.4 K to be well above liquid He temperature; H_{c2} is estimated to be at 7 T.¹⁸

1.4. Diamond Synthesis

The concept of growing synthetic diamond dates back to the 20th century, where initial methods were to mimic nature's way of synthesising diamond by subjecting graphite to high pressures ($p \approx 50$ -100 kBar)

and high temperatures ($T \approx 1800\text{-}2300\text{ K}$) (HPHT). This process was carried out in the presence of a solvent metal catalyst and the solvated carbon was left to crystallise to produce a large single crystal diamond.¹⁹

Albeit the diamond crystals possess the desirable hardness and thermal conductivity properties that replicate natural diamond, the HPHT method is limited to only producing single crystals and this hinders the full exploration of its potential applications. A new method emerged a decade later, which describes the thermal decomposition of carbon containing gas precursors at reduced pressures and subsequent deposition of diamond onto a solid substrate.

The development of the chemical vapour deposition (CVD) technique enabled diamond to be synthesised in the form of films and coatings on various shapes and grain sizes (ranging nm-mm). The surface used for deposition can either be bulk diamond or a non-diamond species. The diamond films grown on bulk diamond are said to be homoepitaxial and single crystalline whilst non-diamond substrates are heteroepitaxial and polycrystalline.⁶

Furthermore, the latter diamond films require an extra nucleation step to encourage spontaneous deposition of diamond on a non-diamond species. There are several seeding techniques which induce CVD growth, and this is discussed in section 1.5.1. The resulting continuous films are polycrystalline, nanocrystalline or ultrananocrystalline in accordance to its average grain size. The grain size and sp^3/sp^2 ratio of the CVD diamond is what determines its macroscopic properties.

1.4.1. Chemical Vapour Deposition (CVD) of Diamond

The general starting mechanism of any CVD technique is the activation of hydrocarbon precursors (usually methane) via thermal-, combustion- and plasma-enhanced methods such as a hot filament or microwave plasma-assisted activation.

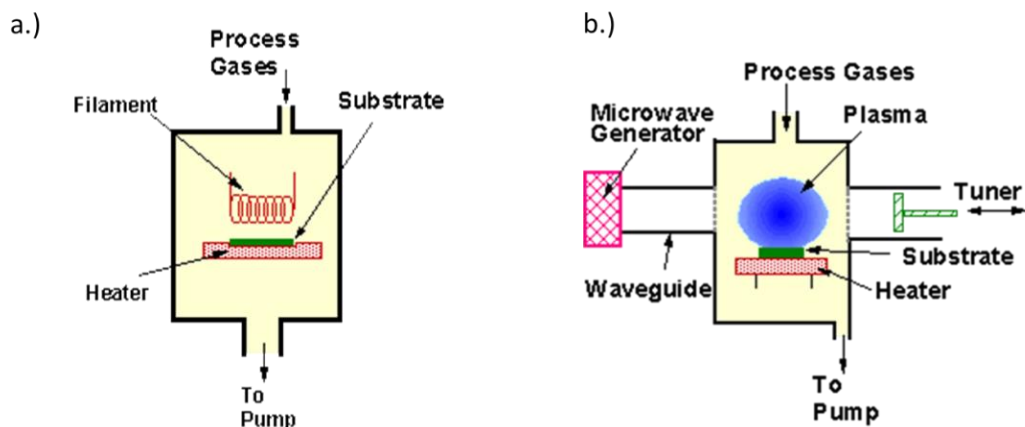
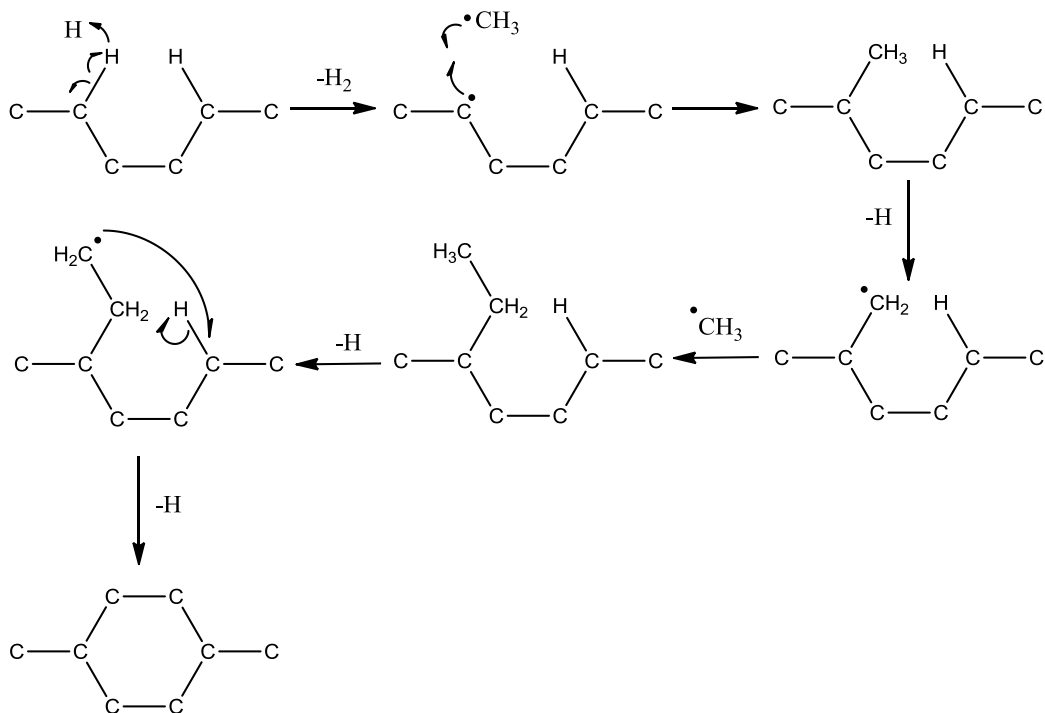


Figure 5. Two common CVD reactors. (a) hot filament reactor, (b) microwave plasma enhanced reactor²⁰

At high temperatures and low pressures (2200-2400 K, 20 Torr), carbon-containing gases diluted in the excess of hydrogen (typically 1:100 for microcrystalline growth) are introduced into the activated gas chamber above a solid substrate. H_2 gas decomposes and carbon-containing radical species are subsequently formed via hydrogen abstraction.²¹ Deposition involves a series of adsorption/desorption processes at the surface.

One suggested mechanism describes atomic hydrogen abstraction of the terminating hydrogen atom to form stronger molecular H-H bonds. The carbon containing radical then adds onto the lattice and the process repeats for the terminal H atom of the newly added carbon species. An internal H_2 elimination follows and ring closure propagates the diamond lattice structure.⁴ Although the process is reversible, the stability of the transition states in the diamond structure is strongly favoured over the graphitic carbon equivalent, thus diamond deposition is driven by kinetic stability of the product.



Scheme 1. Suggested mechanism for diamond deposition through a series of hydrogen abstractions and methyl additions⁴

Growth is usually accomplished in an excess of hydrogen as diamond is more stable towards atomic hydrogen than graphite. This helps etch graphite quicker and enhances removal at surface sites. Moreover, atomic hydrogen has the tendency to become attached to the growth surface and stabilise the sp^3 diamond lattice, thus hydrogen playing a key role in CVD diamond synthesis.

The conditions formulated are generally discussed in terms of Bachmann's empirical phase diagram (Figure 6). The diagram summarises all the different processes that can be encountered during CVD diamond growth. The C, H and O gas compositions are divided into three main categories: no growth, diamond growth, and non-diamond carbon growth.

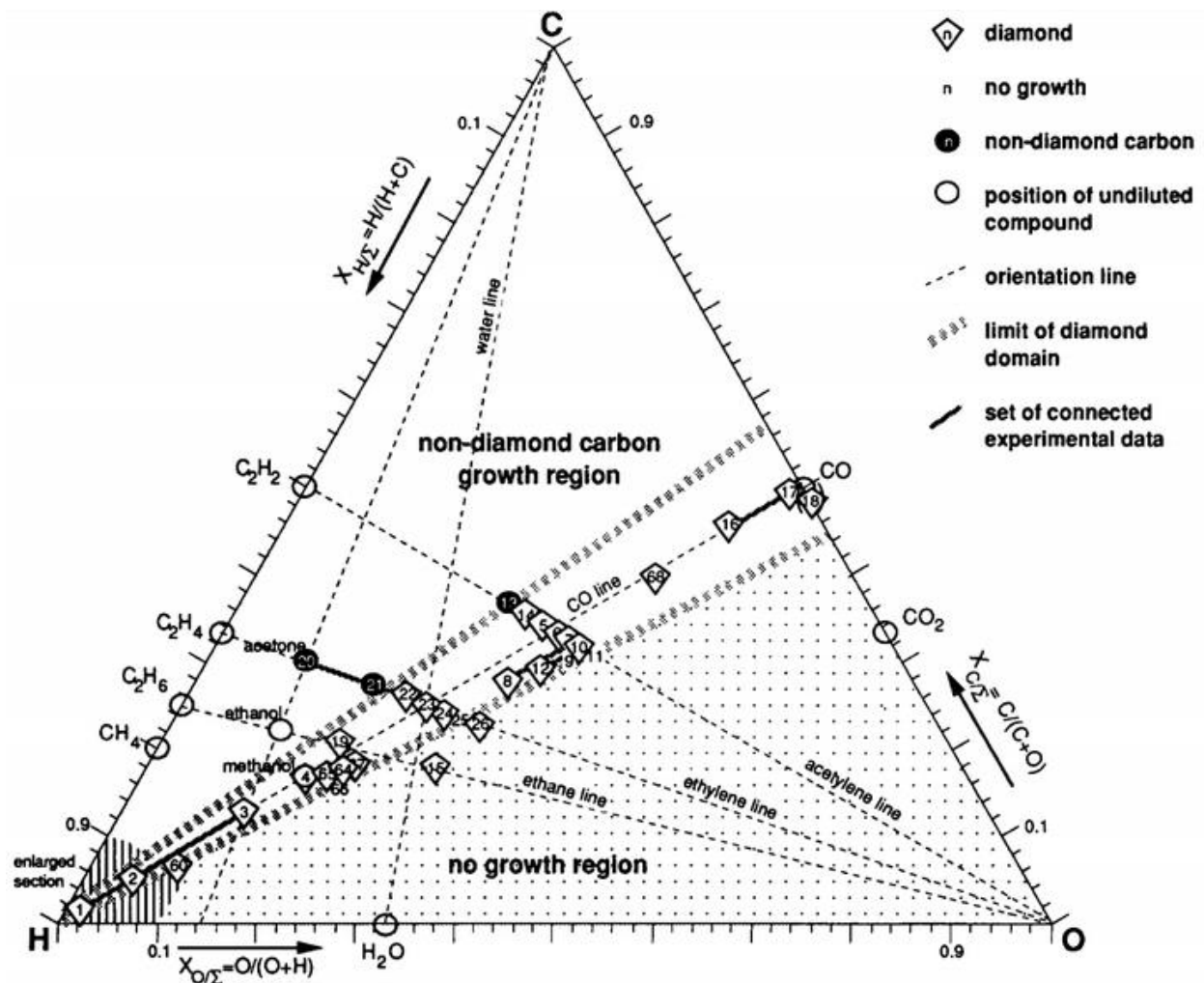


Figure 6. Bachmann's phase diagram for diamond deposition from C/H/O systems²²

The dissociation of precursor molecules requires large activation energies (230-243 kJ mol⁻¹ for methane). To increase the growth rate, activation processes are used to increase the temperature of the reaction chamber to around 900 °C; the hydrocarbons then fragment into reactive radical and atomic species which nucleate and grow onto the substrate surface.

1.5. Nucleation Techniques

Nucleation describes the earliest stages of thin film diamond growth and this is known as the induction period. Nucleation enhancement is heavily dependent on the quality of pre-treatment processes. The abrasion technique involves roughening or ultrasonic agitation²³ of the substrate, which forms "defects" for diamond powder to adsorb. This method increases the nucleation density from about 10⁴ cm⁻² (unscratched substrate) to about 10⁷ particles cm⁻²²⁴ as more surface sites (e.g. kinks, terraces, steps) are created. The interfacial tension between diamond and non-diamond substrates decreases; for

instance, the surface energy of diamond compared to Si (6 J cm^{-2} and 1.5 J cm^{-2} respectively) means a low sticking coefficient prior to surface treatment.²⁵ Nucleation is necessary to induce growth and to compensate for the surface energy mismatch between the two different materials.

Another pre-treatment method describes applying a bias on a conductive substrate under hydrocarbon rich conditions and is typically used in microwave plasma-assisted CVD.²⁶ The sub-plantation mechanism is thought to be incident CH_x^+ ions and $\text{CH}_x\cdot$ radicals coming to the surface, forming a sp^3 bonded layer under high substrate temperatures. The in-situ technique yields a nucleation density of about 10^{10} cm^{-2} but it has a disadvantage of the requirement of conductive and high melting point substrates.²⁷

The most adaptable method is seeding the substrate with diamond particles and subsequently initiating diamond growth homoepitaxially. Early approaches involved coating with larger sub-microscale diamond particles known as diamond grit, but smaller nanodiamond can now be obtained by ultra-milling and detonation processes. This technique yields very high nucleation densities; it is also the least substrate damaging, works at ambient temperatures and the surface chemistry can be easily tuned. Thus this will be the main technique discussed in further sections of this report.

1.5.1. Seeding Methods

For an even coverage of diamond nanoparticles onto the substrate surface, the coating is best done if the particles are in the form of suspension. The suspended particles can be deposited onto the substrate by drop casting followed by evaporation of the solvent. However, this method does not lead to homogeneous deposition due to convection forces and possible aggregation in more concentrated regions.

To overcome this, homogeneous dispersion can be accomplished by spin coating and the speed of rotation can effectively dry the suspension. An example of spin coating is demonstrated by electrostatic spray deposition (Figure 7). The sample substrate is stuck on a rotary mount using conductive sticking pads and spins inside an insulating box. A metal syringe containing the colloidal suspension is positioned relative to the centre of the substrate; a high voltage is then applied and the sample is pulled through the syringe.

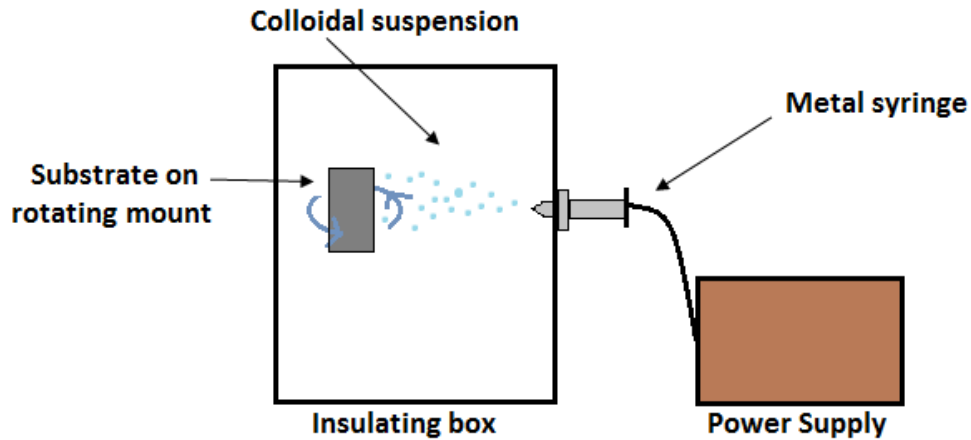


Figure 7. Schematic of electrostatic spray deposition

The diamond suspension can either be prepared in buffer for electrostatic stabilisation or in a polymer solution for self-assembly (see section 2.3); a combination of the two is also used.

1.6. Boron Doped Nanoparticles

Diamond nanoparticles have found uses in many areas of nanotechnology, from cellular biomarkers and quantum computing, to hard coatings and composites.²⁸ Nanodiamond (ND) particles are conventionally made by detonation synthesis or a bead milling process where HPHT or CVD microcrystalline diamonds are ground down to nanosize particles (top-down method). The resulting ND particles can be used as seeds for substrates to create nucleation sites for CVD diamond growth.

The choice of diamond powders depend upon the desired surface chemistry. For example a bead milled, boron doped nanocrystalline diamond powder is selective of inducing conductivity.

If the desire was to create BDD films, it may be important to ensure the entire film is conductive, including the particles at the diamond-substrate interface. This is because undoped seeds such as detonation nanodiamond (DND) powders create an insulating layer which becomes a significant problem for materials in nanoscale thickness.²⁹

BDD thin films can also be obtained by *ex situ* doping via ion implantation. This method uses high energy ion bombardment where the ions are accelerated in an electric field and enters the target solid at controlled penetration depth. Diamond has small interatomic spacing (C-C bond length 1.54 Å) and this means the rigid lattice is highly resistant to implantation. Thus the need for even higher energy

impact ions can be destructive to the diamond surface. The crystal lattice can become damaged and reconstruction of the surface due to energy minimisation can lead to undesirable graphitization.

Moreover, depending on the depth of implantation, the method may not be a solution to the undoped layer problem. Depending on the surface morphology, the different types of diamond facets can affect the depth distribution of ions. For example, if the ions travel in the (110) direction of the diamond cubic crystal lattice, they can penetrate at a longer range than the (100) direction. This is because of the open axial ion channels present in the former facets, which reduce the resistance and hence facilitate ion channelling.³⁰ To achieve uniform and effective implantation, the diamond substrate must therefore require high preferential orientation of ion centres along particular directions.

A thin layer BDD coating can be grown onto a non-diamond substrate surface at high temperatures in a CVD reactor (bottom-up approach). The drawback of this method is in the absence of seeding, the initial growth rate during the induction period is impractically slow. Moreover, the limited choice of high melting point substrates means that there is a threshold towards increased growth temperatures.

Subsequently there has been an increased interest in using doped seeds created via a top down approach. Recently some attempts by Janssen have been made on BDD coating via self-assembly of BDD particles.³¹ The BDD was bead milled and purified; the particles were then centrifuged to separate size distribution, and were suspended in a suitable medium which allows effective self-assembly on the substrate to take place.

2. The Diamond-Substrate Interface

During self-assembly, for the diamond- substrate interface to be successfully conducting there must be a good coverage of doped nanodiamond particles which are in contact with one another to form an electrical pathway. There are several things which need to be considered to ensure this:

- 1.) There must not be a broad particle size distribution of diamond at a particular interface
- 2.) The diamond must not be contaminated with any insulating particulates such as quartz or alumina powder
- 3.) The substrate and the particles need to have opposing charges as formation of a monolayer is predominantly induced by electrostatic attraction
- 4.) The diamond particles must not agglomerate in the suspension to ensure an even coverage

2.1. Particle Size Separation

The bead milling process involved the pulverising of a CVD free-standing polycrystalline BDD provided by Element Six. These crystals were around 200 μm in size and the top-down approach aims to grind the particles down to nanoscale.

Inevitably there would be a broad particle size distribution and, as has been reported in the literature, there has been little or no attempt to accurately separate out the particles. The general method this has been done is via centrifugation,³⁹ but even so this technique only provides slightly narrower distributions thus particle size separation remains to be a challenge.

2.2. Acid Treatment for Impurity Removal and Oxidative Removal of sp^2 Carbon

The grinding balls used for bead milling tend to be made of zirconia or steel, and under high impact pulverising, the diamond material may undergo contamination as the harder diamond causes abrasion of the balls. When steel balls are used, the iron component can easily be removed with hydrochloric acid at elevated temperatures ($> 200^\circ\text{C}$). Nanoscale zirconium is more difficult to remove, however it can be achieved. Liang et al. has reported the treatment of zirconium with phosphoric acid for extended periods of time followed by chromatographic separation.³²

As well as impurity removal during milling, there is another problem which arises. Dangling bonds generated at the diamond surface may cause graphitisation where the sp^3 carbon reconstructs to form the more thermodynamically stable sp^2 graphitic structure. To prevent this, diamond can be cleaned by

powerful oxidising agents such as a boiling mixture of sulphuric acid and potassium nitrate³³. This carboxylation treatment removes the sp^2 carbons in the lattice and could further remove any metallic impurities generated from abrasions. It also provides an oxygen terminated diamond surface which could act as an insulating layer for electronic devices.

It is possible to polish diamond nanoparticles with diamond grit. However, the mechanism is not fully known and polishing can only be achieved on certain surfaces and in certain directions. One explanation for such behaviour is that the polishing movement dislodges the atoms at the surface and forms an amorphous layer. The carbon atoms are either loosely bonded or tightly packed to the lattice below and this determines whether it will be polished off or not.³⁴

2.3. Preparing a Stable Diamond Suspension

There are three key parameters to consider for a stable colloidal suspension: viscosity, particle size and zeta potential. By increasing the viscosity or decreasing particle size, the rate of aggregation and sedimentation slows and this is a form a kinetic stabilisation. On the other hand, inducing steric and electrostatic stabilisation is a thermodynamic property.

Particle size becomes more significant when it is above the sub-micron scale. Gravitational effects outweigh Brownian motion and the stability of the suspension is governed by reducing the density difference between the medium and particles.

Electrostatic stabilisation prevents agglomeration by inducing repulsive forces between the particles. One method of doing this is by increasing charges opposing the surface charge of the particles. The electrokinetic potential in colloidal suspensions is a measure of stability and it can be measured by zeta potential analysis. A nanoparticle forms an electric double layer where the surface charge attracts ions of the opposite charge to form two layers of ions (Figure 8). The electrical potential at the boundary is the zeta potential, and it is the potential between the stationary layer and the bulk layer. If the absolute value is larger than $|30|$ mV, the electrostatic forces are said to be favourable and typically have high stability.

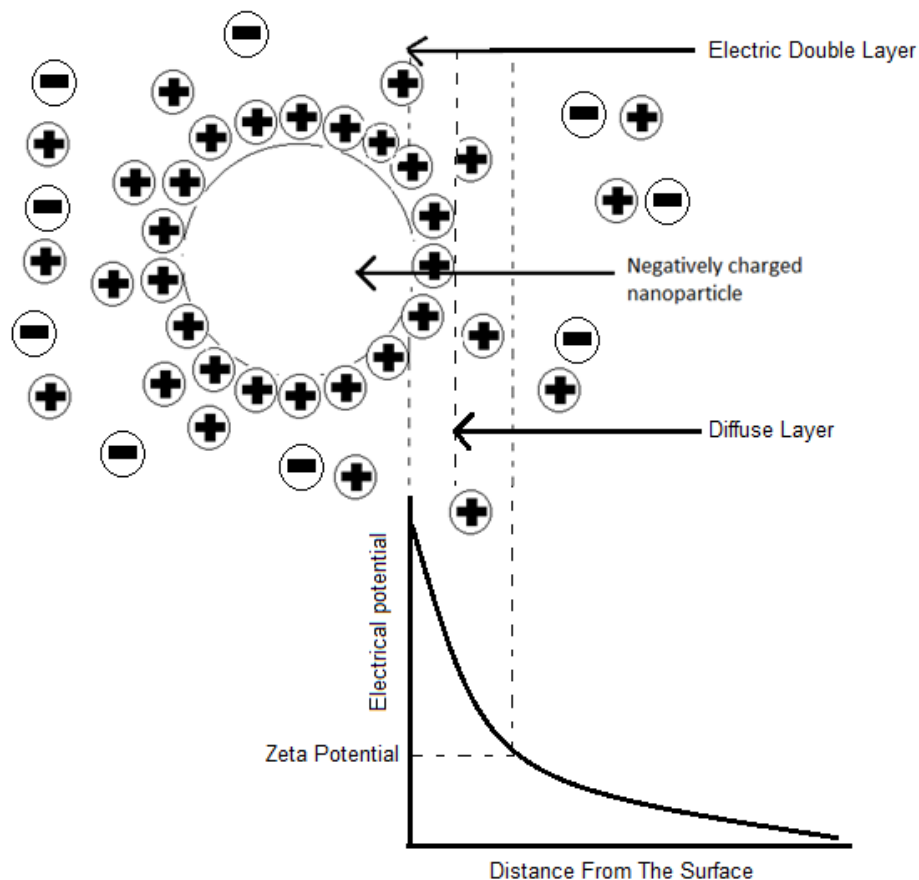


Figure 8. Schematic diagram of the electric double layer and zeta potential

After undergoing oxidative acid treatment, the diamond carbon layer is surface terminated by oxygen, and thus mainly consists of carboxylate and alcohol groups. The polar groups would result in a surface charge and the charge sign is dependent on the pH of the medium. At pH 4 and above, the deprotonated form gives a negative zeta potential.³⁹

On the other hand, the substrate is also negatively charged due to the native oxide layer. As mentioned, opposite zeta potentials of magnitude [30] mV yield good suspension stability, hence surface modification is necessary to either diamond or substrate for achieving successful self-assembly.

The diamond particles have to be suspended to a medium for seeding thus at first instance it may seem sensible to carry out surface modification on the diamond particles. One fabrication method is coating the nanodiamond with positively charged groups e.g. NH_4^+ groups in a cationic polymer solution, such as poly(ethylenimine) (PEI); the structure is shown in (Figure 9). As well as inducing electrostatic attraction between diamond and substrate, the polymer solutions can also prevent coagulation of the diamond particles by providing steric bulk and repulsive charges at the surface. Surface modification on the

substrate with positively charged groups is another feasible method; the diamond can be suspended in an alkaline buffer solution for increased negative zeta potential and hence stabilisation.

2.3.1. Surface Modification of Boron Doped Diamond

The zeta potential becomes positive when the diamond particles are suspended in a cationic polymer solution. This increases the electrostatic attraction with the negatively charged substrate. Coating the substrate with a negative polymer solution, such as poly(sodium 4-styrenesulfonate) (PSS) may also enhance the attraction with the diamond suspension; the structure is shown in (Figure 9). The diamond nanoparticles are seeded via a polymer self-assembly method (Figure 10).

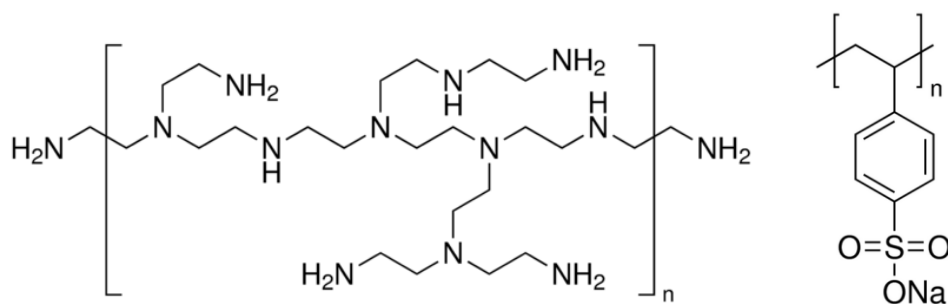


Figure 9. Chemical structures of branched PEI (left) and PSS (right)

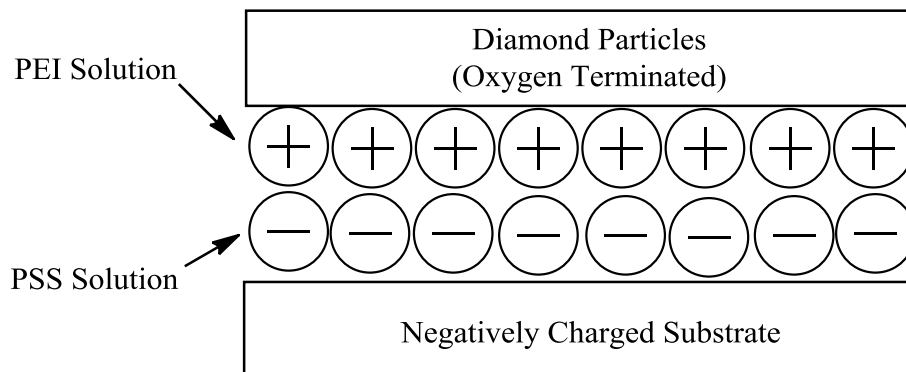


Figure 10. Diamond seeding via polymer assembly. The addition of polymer provides steric stabilisation to prevent coagulation, and also induces electrostatic attraction of the opposing surface charges

2.3.2. Surface Modification of Substrate

The negative zeta potential of diamond can be enhanced by increasing the pH of the suspension. By using an alkaline buffer solution and maintaining a high pH, the diamond particles become highly negatively charged. The substrate is then coated with a cationic polymer to induce electrostatic attraction and effective adhesion (Figure 11).

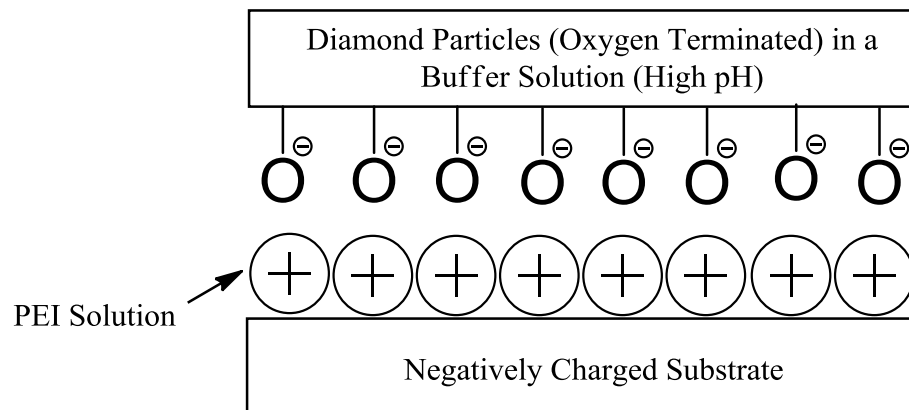


Figure 11. Diamond seeding via electrostatic attraction

It has been reported that positive zeta potential of nanodiamond can be achieved by hydrogenating the nanodiamond by hydrogen or vacuum annealing³⁵. The reductive treatment is based on the reaction of the sp^2 diamond matrix with hydrogen and the zeta potential is positive for all pH ranges.

Polarisation of the substrate and cathodic electrophoretic seeding of diamond particles have also been investigated by Zhitomirsky et al.³⁶ However these techniques have not been fully explored and polymer chemistry has been the most effective charge modification technique to date.

2.3.3. The Choice of Substrate

The choice of substrate determines the outcome of diamond type after CVD growth. For example, the substrate needs to be diamond in order to achieve a single crystal diamond, but a non-diamond substrate is used to create a polycrystalline CVD diamond.

Deposition on non-diamond substrates usually requires a refractory metal to be chosen as the substrate, which can not only withstand the harsh CVD conditions (i.e. temperatures typically above 750 °C) but is also able to form a stable thin carbide layer at the interface. The carbide layer provides an “adhesive” layer by partially relieving the effects of thermal expansion and promotes even growth. However, a substrate that has too high an affinity to react with carbon such as Pd and Ni would cause the carbon to solubilise and enter the bulk of the substrate. Materials such as Si, Mo and W can form localised carbide layers at the surface which provides adhesion for subsequent CVD growth.

Other desirable features of CVD substrates are high melting points and low coefficients of thermal expansion. The substrate needs to withstand the growth temperature conditions of the reactor and the coefficient of thermal expansion must not be vastly different with diamond. Diamond has a very small

expansion coefficient whilst the substrate will expand upon heating and contract upon cooling. If the mismatch is significant the product will undergo cracking and delamination upon cooling. However, this can be an ideal method for growing free-standing diamonds, and some of the ideal candidates are Sn, Pb, Au and Ag. The thermal expansion coefficients of various materials are shown in Figure 12.

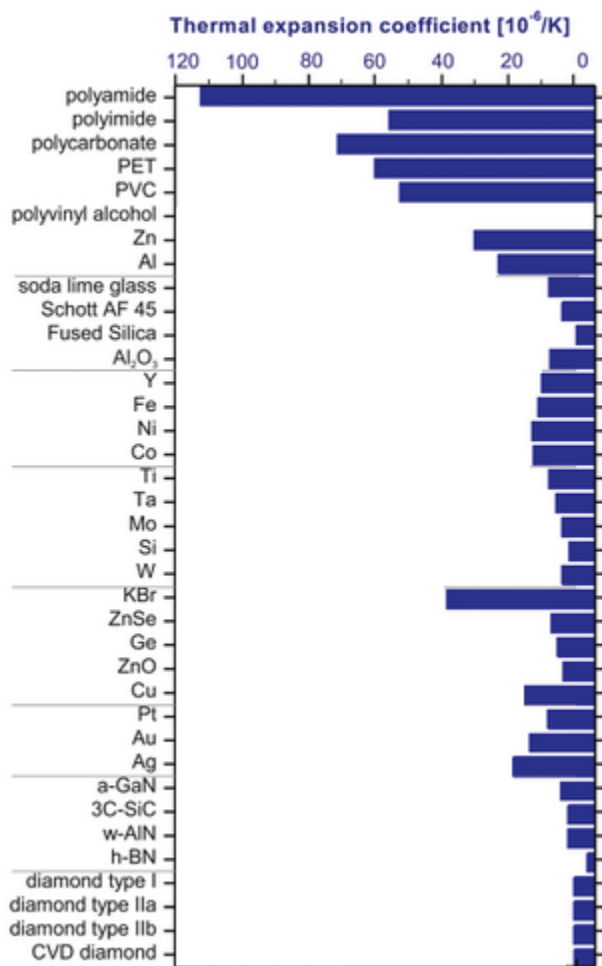


Figure 12. The thermal expansion coefficients of various substrates (adapted from reference)³⁹

2.4. Mechanical and Chemical De-agglomeration

Nanoparticles generally agglomerate via the accumulation of non-covalent interactions such as Van Der Waals and coulombic interactions between particles. This is undesirable as it destabilises the colloidal suspension and overall causes an uneven coverage of the surface.

It is known that DND is susceptible to agglomeration. DND is formed via both non-covalent and covalent interactions between individual particles. This is due to highly reactive surface groups that undergo bond formation when the aqueous suspension is dried away.³⁷

To avoid agglomeration, mechanical methods such as attrition milling³⁸ and sonication are necessary. Chemical methods such as hydroxylation³⁸ or oxygen termination at the surface can induce repulsive forces and separate the particles.

2.5. The CVD Diamond Film

Seeding the substrate provides nucleation sites for subsequent CVD growth. The quality of the seeded substrate, hence the level of success of the self-assembly technique, can be assessed by studying the diamond film after CVD growth.

Ideally a monolayer of nanodiamond particles is formed on the substrate after self-assembly, but this is often not the case. This could be for many reasons. The magnitude of zeta potential could be too low to give a stable suspension; the particle size distribution could be too high resulting in faster sedimentation for larger particles; agglomeration may result in uneven coverage and different layer thicknesses.

If the substrate was poorly seeded, it would be difficult to study and characterise due to poor nucleation density. By using the CVD technique, growth occurs on the nucleation sites in three dimensions. To begin with, the crystals are of various sizes depending on the number of seeded diamond nuclei in a given area, these crystals are described as “islands”. As growth continues upwards and out, the small islands get bigger and interact with neighbouring crystals, thus slowly forming a continuous film. The resulting thin film is polycrystalline and has many defects and grain boundaries.

By altering the time of exposure to CVD conditions, different properties can be studied. At minimal exposure time, the crystal size increases and facilitates the determining of nucleation density. At longer exposure times, the surface morphology can be studied and also surface conductivity.

2.6. Project Aims

The use of boron doped diamond nanoparticles as seeds for nucleating BDD thin film growth has many attractive applications. Notably, the elimination of the insulating seeding layer present in conventional methods is of distinctive interest. The incorporation of higher boron content at the diamond-substrate interface can be marketed for electronic and electrochemical applications.

Fundamentally, in creating a homogeneous BDD film, the chemical and physical properties of BDD nanoparticles can be fully explored. The surface morphology can be studied with SEM, and the orientation of the boron atoms within the crystal lattice can be studied using TEM or AFM, for example.

It is a reasonable assumption to suggest the undoped seeded layer contains non-conductive regions in the full film. However, it is important to assess the true significance of the undoped layer and to what extent it varies with doped seeds in terms of conductivity and other electronic properties. It would also be interesting to investigate whether different seeds can modify the deposition growth rate and the morphology of the resulting film.

2.7. Applications

2.7.1. Diamond Electrodes

An electrode is a conductor which carries electrical charge via the transport of ions. Electrochemical sensors are applicable for many aspects of fundamental research and in the industry. This broadly ranges from batteries and fuel cells to biological aspects such as blood glucose detection.³⁹

BDD electrodes can be advantageous over conventional electrodes; they exhibit a relatively low signal-to-background-current ratio due to their relatively small double layer capacitance ($\sim 10 \mu\text{F cm}^{-2}$) and a lower density of ionisable or redox active groups on the surface. This removes any extra background peaks normally present in typical electrochemical data.

Moreover, diamond is chemically inert to most materials thus provides a wide potential window with the width of 3-4 V in aqueous and 5-7.5 V in non-aqueous media.⁴⁰ The potential window can be described as the range between the onset of hydrogen evolution (current rise at negative potentials) and oxygen evolution (current rise at positive potentials).

Polycrystalline, oxygen terminated, BDD electrodes were recently reported by Hutton et al., which supported heterogeneous electron transfer (HET) for $\text{Fe}(\text{CN})_6^{4-}$ electrolysis. A hydrogen terminated surface was unstable to electroanalysis as the potential increased, and the HET rate decreased upon being subjected to successive potential cycles. Oppositely, an oxygen terminated surface under specific oxidation methods, produced stable cyclic voltammetry responses over repetitive cycles.⁴¹

2.7.2. Low Melting Point Substrates

The BDD nanoparticles have unique surface chemistry and improved selectivity. DND powder is insulating and undoped, whilst BDD is boron doped and conductive. Until last year, nanocrystalline diamond particles with homogeneous boron doping had not been reported.²⁹ By creating a BDD suspension, various coatings can be accomplished without having to undergo the harsh conditions of

CVD processes. This opens a platform for a wider range of applications, such as a new generation of electrodes on glass and low melting point materials.

2.7.3. Surface Termination and Electron Affinity

At the surface of diamond, there are sp^3 carbon orbitals which point outwards and have an unpaired electron. This orbital is also known as a “dangling bond”, and in order to minimise the high energy states, they either reconstruct at the surface by pairing up with other dangling bonds, or they bond to other atoms at the surface and initiate termination. These atoms could be hydrogen, oxygen or alkali metals such as sodium and lithium.

The electrostatic forces between the carbon and terminating species can change the electronic properties at the surface and effectively the bulk as well. The dipoles induced do not have a net charge but the energy barrier of electron emission alters with respect to the direction of the dipole.

The electron affinity χ is defined as the energy difference of the electrons in the bottom conduction band (lowest unoccupied state) relative to the vacuum level. The work function Φ determines χ and in a non-degenerate semi-conductor the Fermi level sits within the band gap and therefore $\Phi > \chi$. As described in section 1.3.1, band bending affects the Fermi level which in effect modifies Φ , but χ remains unchanged. However, χ is influenced by the charge polarisation of the heteroatoms at the surface, and thus the efficiency of electron emission from the conduction band minimum to the vacuum level can be governed by the terminating species of the diamond.

If the terminating species is hydrogen, the resulting electron affinity is negative, indicating the electrons at the conduction band minimum are higher in energy than the vacuum level due to carbon being more electronegative than hydrogen. This means that any of these electrons can enter the vacuum level and emit to the surface with zero energy barrier (Figure 13).

Negative electron affinities (NEA) of diamond surfaces provide low temperature emission and low work function Φ of materials. This is very useful for thermionic and high electron field emission applications, such as thermionic energy converter devices used to generate electricity. Thermal energy sources include solar, geothermal and nuclear and thus such converters can provide a new generation of renewable energy resources.⁴²

More recently, there have been some empirical and theoretical studies on the termination of diamond surfaces with metal oxides. These surfaces exhibit NEA values that are significantly higher than those

resulting from hydrogen termination. Moreover, they are relatively stable up to 1000 K. Currently, the most promising metal oxide being LiO, but other candidates such as MgO, TiO, TaO and VO are also being considered.⁴³

Conversely, if the terminating species is electronegative, such as oxygen, the vacuum level would be higher than that of the conduction band. This could be explained by the electron rich surface repelling other electrons from going near the bulk, thus preventing electron emission into the vacuum. This results in a positive affinity surface of diamond (Figure 13).

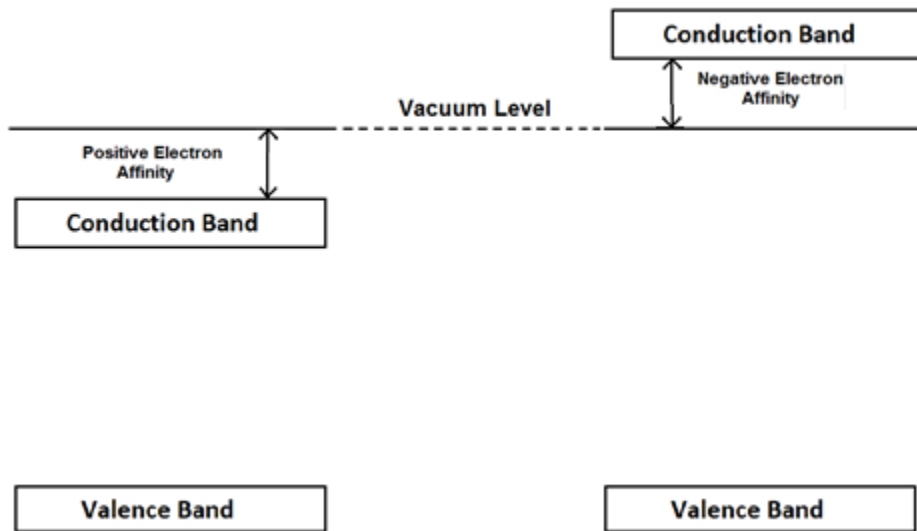


Figure 13. Schematic illustrating the effect of termination atoms on electron affinity. A more electropositive terminating species give rise to NEA whereas a more electronegative termination species give rise to PEA

In a p-type semiconductor, the downward band bending lowers the work function and electron affinity. At high enough surface potential, the electron affinity can effectively reverse from PEA to NEA. In this example, the bottom conduction band lies above the vacuum level initially as most semiconductors do. But as the dopant level increases, the Fermi energy decreases with χ and the downward band bending increases, thus inducing NEA and lower Φ .⁴⁴ In summary, both the surface termination and dopant concentration can alter the electron affinity of the semiconductor material.

3. Experimental

3.1. Materials

The polycrystalline BDD samples were manufactured by Element Six. The PEI polymer solutions were manufactured by Sigma Aldrich. The as purchased BDD was 10 × 10 mm, 0.6 mm thick. The resistivity was 0.02 – 0.18 Ω.cm and the boron concentration was $> 10^{20} \text{ cm}^{-3}$.

3.2. Preparation

3.2.1. Bead Milling

The HPHT diamond samples were bead milled with steel beads at a rate of 20 Hz for 7 hours. Steel beads are known to coat diamond very well; this coating effectively pulverises diamond with itself and thus enables a more efficient process. The steel beads were washed consecutively with 50 mL de-ionised water, acetone, methanol and ethanol (10 minutes sonication per wash) and were then dried using compressed gas. The sample was placed between two beads in the grinding jar of the Mixer Mill MM200 (Retsch) and after milling the resulting diamond had homogenised into a grey fine powder.



Figure 14. Grinding jar and steel beads

3.2.2. Acid Treatment

On a hot plate at 120° C, a solution of 100 mL H₂SO₄ (95% w/v) and 6.5 g KNO₃ was slowly added into a round bottomed flask containing the diamond powder. A dark grey suspension formed instantly. Yellow fumes started to appear as nitrogen dioxide was formed and the suspension was left under reflux for 30 minutes.

Once cooled, the solution was neutralised with de-ionised water, and later with KOH (5 mol dm⁻³). The solution was left to settle and was then separated into two columns by pipetting the top layer which contained the lighter diamond particles. Both columns were centrifuged for 5 minutes then a further

30 minutes to separate particle size; four solutions yielded in total and all liquid contents were evaporated, leaving behind finely powdered, oxygen terminated boron-doped diamond. The following sample fabrication methods were carried out with the finest of the four samples only.

3.2.3. Sample Fabrication – Seeding Methods

3.2.3.1. Substrate/BDD in Polymer

Three types of branched poly(ethylenimine) (PEI) solutions (PEI 1-3) were used to prepare a stable diamond suspension. pH studies were also carried out briefly to examine its effects on the stability of the suspension. The acidity of the PEI solution was increased with 10 wt% acetic acid and the zeta potential was determined.

PEI 3 (2 mL, 5 wt% in de-ionised water) and BDD particles (0.005g, 0.25 % w/v) were sonicated for 7 hours and left to stand. The suspension was stable for longer than 48 hours. PEI 1 and PEI 2 were stable for < 2 hours and were discarded. Zeta potential measurements were taken for PEI and BDD/water; DLS measurements were taken for the diamond suspension (see sections 3.3.1 and 3.3.2).

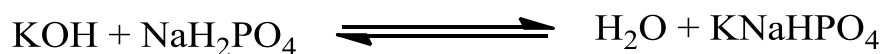
Table 2. PEI solutions under investigation

PEI Sample	Number Average Molecular Weight $M_n / g \text{ mol}^{-1}$	Duration of Suspension Stability
1	600	< 30 minutes
2	1200	< 2 hours
3	60000	> 48 hours

The suspension was drop casted onto a p-type (100) Si substrate labelled substrate A and left to stand for 15 minutes. Substrate A was washed with de-ionised water and dried with compressed air. The substrate was annealed at 300 °C for 1 hour to decompose the polymer and then grown for 5 minutes in a HFCVD reactor using the conditions described in section (3.2.4). SEM images were taken for substrate A.

3.2.3.2. Polymer on Substrate/BDD in Buffer

An alkaline KOH / NaH_2PO_4 buffer solution (pH 8.6, 0.5 mol dm^{-3}) was used to prepare a 2 mL of 0.25 % w/v diamond suspension. The buffer was diluted down with de-ionised water (~ 100 mL) in order to maintain a high pH with minimal impurities.



$$k_a = 2.51 \times 10^{-9} \text{ mol dm}^{-3}$$

Scheme 2. Alkaline buffer system. The k_a value suggests that equilibrium lies on LHS

At a high pH, the oxygen terminated diamond surfaces become highly negatively charged and this enhances electrostatic attraction with the PEI solution. PEI 3 (5 wt% in de-ionised water) was drop casted onto three p-type (100) Si substrates and left to stand for 15 minutes. The substrates were then washed with de-ionised water and the diamond/buffer solution was drop casted immediately after sonication. After 15 minutes, the substrates were washed, dried and annealed at 300 °C for 1 hour as described in the previous section. The substrates were named Substrate B1, B2 and B3 respectively; all substrates' pre-treatment conditions were identical prior to CVD growth.

The diamond / buffer solution was not stable during the drop casting step. The method did not account for sedimentation effects which may occur during the polymer self-assembly step. Sedimentation could lead to an uneven coverage and a tendency to deposit larger, heavier sized particles at a faster rate.

B1 was placed under a HFCVD reactor for 1 hour using highly boron doped conditions, B2 was grown under low dopant concentration for 1 hour, and B3 was grown for 30 minutes at high boron concentration. The CVD conditions are described in section (3.2.4). Samples were characterised using SEM before and after growth. Resistance measurements were taken for all samples using an ohmmeter to measure the conductivity across and through the substrate after growth (Section 3.3.4).

3.2.3.3. Substrate/BDD in Buffer

A diluted KOH/ NaH₂PO₄ buffer solution (pH 8.6, 0.5 mol dm⁻³) was used to prepare a 50 mL stable diamond suspension at 0.005 % w/v. The solution was sonicated for 30 minutes and the suspension was stable for 3-4 hrs. 30 mL was taken from the top of the solution which remained stable for a further 1-2 hours; the remaining solution containing remnants of sedimentation was discarded. Zeta potential and DLS measurements were taken (see sections 3.3.1 and 3.3.2).

Results show a positive zeta potential for the diamond/buffer suspension (see 4.3) and thus at this point, adhesion to the negative substrate was assumed to be spontaneous and not facilitated by polymer addition. Three Si substrates, labelled substrate C1, C2 and C3 respectively, were submerged in suspension and left to stand for 30 minutes.

In order to investigate more ways of optimising the seeding method thus increasing nucleation density, the three substrates were prepared as follows:

Substrate C1: The suspension was washed with de-ionised water and dried with compressed air.

Substrate C2: The suspension was washed with de-ionised water, dried with compressed air and then re-submerged into the suspension for a further 1 hour; total exposure time to the BDD suspension was 1 hour 30 minutes.

Substrate C3: The suspension was washed with de-ionised water, dried with compressed air and re-submerged into the suspension for 1 hour. This step was repeated 3 more times; total exposure time to the BDD suspension was 4 hour 30 minutes.

SEM images were taken for substrates C1 and C3 prior to CVD growth. C3 was grown under high boron dopant conditions for 1 hour (section 3.2.4). Resistance measurements were taken for all samples using an ohmmeter to measure the conductivity across and through the substrate after growth (Section 3.3.4).

3.2.3.4. Substrate/Undoped Seeds

As well as optimising the seeding/ nucleation method for enhanced growth and better adhesion, results must be compared to those of undoped seeds in order to investigate whether doped seeds do indeed enhance conductivity across the diamond/substrate interface and to what extent.

The self-assembly was on a p-type (100) Si as before. A solution of DND (20%) in carboxyethylsilanetriol sodium salt solution (25 %w/v) was drop casted onto three substrates, labelled Substrate D1, D2 and D3 respectively. Carboxyethylsilanetriol contains inorganic silane functional groups which, when coated onto the nanodiamond particle surface, prevents agglomeration of the particles.⁴⁵ The samples were left to stand for 15 minutes before it was washed with de-ionised water. The nanodiamond particle size was quoted 18 nm from the manufacturer but DLS revealed the true size to be 36 nm.

D1 was grown under high boron dopant conditions for 1 hour, D2 was grown under low boron concentration for 1 hour and D3 was grown under high boron concentration for 30 minutes. The CVD conditions are described in 3.2.4. D1 was characterised using SEM and Raman spectroscopy after CVD growth. Resistance measurements were taken for all samples using an ohmmeter to measure the conductivity across and through the substrate after growth (Section 3.3.4).

The conditions of all A, B, C and D substrates are summarised in Table 3.

Table 3. The conditions of A, B, C and D substrates

Substrate	Self-assembly method	Self-assembly time	CVD conditions
A	Substrate/ BDD in polymer	15 minutes	High [B], 5 minutes
B1	Polymer on substrate / BDD in buffer	15 minutes	High [B], 1 hour
B2	Polymer on substrate / BDD in buffer	15 minutes	Low [B], 1 hour
B3	Polymer on substrate / BDD in buffer	15 minutes	High [B], 30 minutes
C1	Substrate / BDD in buffer	30 minutes	-
C2	Substrate / BDD in buffer	1 hour 30 minutes	-
C3	Substrate / BDD in buffer	4 hour 30 minutes	High [B], 1 hour
D1	Substrate / undoped seeds	15 minutes	High [B], 1 hour
D2	Substrate / undoped seeds	15 minutes	Low [B], 1 hour
D3	Substrate / undoped seeds	15 minutes	High [B], 30 minutes

3.2.4. CVD Diamond Growth

A diamond film was grown onto the seeded Si substrates in a standard hot filament CVD reactor using CH₄/H₂ process gases at a pressure of 20 Torr. B₂H₆/H₂ (5% B₂H₆) was used as the B precursor and Ta was used as the filament in the HFCVD process. The filament temperature was kept constant at 2400 °C and the substrate temperature was maintained at 900 °C. Substrates were grown in either of two conditions: at high boron concentration or at low boron concentration. The gas flow rates were monitored using mass flow controllers (MFCs).

In order to obtain highly doped substrates, the concentrations were 1.24% B₂H₆/CH₄ and 1% CH₄/H₂ gas. In order to obtain relatively low boron doped samples, the concentrations were 0.22% B₂H₆/CH₄ and 1% CH₄/H₂ gas. Table 4 summarises the standard gases used in this study, MFC offset of the respective gases, volume of gas recorded on the MFC controller in standard cubic centimetre per minute (sccm) and concentration of each gas relative to H₂ or CH₄ atmosphere.

Table 4. Summary of the standard gases used and the respective offsets and relative concentrations

Standard Gas	MFC offset	Volume of Gas Recorded / sccm	Percentage relative to H ₂ or CH ₄ / %
H ₂	-4.0	200.0	-
CH ₄	-0.5	2.0	1.00 relative to H ₂
B ₂ H ₆	-1.6	0.1 / 0.5	0.22 / 1.24 relative CH ₄

It is worth noting the boron concentration is non-exact because B is known to diffuse into the reactor and diffuses out again during subsequent growths. It is inevitable that any growing film in the boron-contaminated reactor will be slightly boron doped even if there is no diborane gas flowing through the inlet valve, this is known as residual doping.

After the set growth time, the flow of diborane and methane was stopped and the hydrogen was left to flow for a further 5 minutes. This step enables hydrogen termination at the surface in order to prevent reconstruction driven by the high reactivity of the dangling bonds.

3.3. Characterisation

3.3.1. Dynamic Light Scattering (DLS)

DLS is a method of measuring particle size, particle size distribution and the polydispersity of particles in the suspension. A monochromatic beam hits the sample, and the intensity of scattered light is measured as a function of time. A stationary molecule has a constant amount of scattered light. However, all molecules in solution are subject to Brownian motion and thus the light intensity is relative to the constructive or destructive interference caused by this motion.

Smaller molecules diffuse faster than larger molecules thus the intensity change will be faster. The timescale of the intensity fluctuations is directly proportional to Brownian motion and thus particle size information can be acquired. The temperature and viscosity of the solvent will also affect the fluctuation rate, but these factors are kept constant in order to differentiate particle size.

The particle size changes as a function of pH; the ionic impurities increase the ionic strength thus the screening effect increases; the Debye length decreases as the charges come together and this causes the particles to agglomerate.

The diamond particles were prepared in a stable suspension in order to eliminate gravitational motion (section 3.2.3). As the suspension was prepared in a polyelectrolyte solution, small counterions dissociate and neutralise surface charge on the diamond particles. However, a high polymer concentration increases the ionic strength and has adverse effects. The suspension was sonicated for 15 minutes to remove any potential agglomerates and particle size was measured using a Nano Series Zetasizer S90 (Malvern Instruments) capable of determining nanosized particles down to 0.3 nm. For each sample, three measurements were taken per run and repeated to obtain an average of six results.

3.3.2. Zeta Potential

Zeta potential analysis is an electrophoretic light scattering method of measuring surface charge of particles in solution; the particle size or molecular weight does not necessarily have to be known which is useful. An electric field is applied to the sample and the particles move at a velocity relative to its zeta

potential. The velocity is measured using a patented phase analysis light scattering method (M3-PALS, Malvern Instruments) and the electrophoretic mobility thus zeta potential can be calculated.

The velocity is dependent on the dielectric constant and the viscosity of the medium and zeta potential. Zeta potential is a function of Debye length and is expressed in terms of Henry's function $f(\kappa a)$. In aqueous, polar media (e.g. water) and moderate electrolyte concentration, the Debye length is smaller than the particle diameter size. $F(\kappa a)$ is 1.5 in this case and this is known as the Smoluchowski approximation.

Again, it was necessary to prepare a stable suspension as particle sedimentation can generate undesirable electrokinetic effects thus cause misinterpretation of electrophoretic mobility. The sample was sonicated for 15 minutes to remove any potential agglomerates. Disposable folded capillary cells (DTS1070, Malvern Instruments) were used and the sample was slowly injected into the cell to avoid air bubbles.

Zeta potential was measured using Zetasizer Nano Z (Malvern Instruments) capable of determining zeta potential in both polar and non-polar media using the Smoluchowski or the Huckel approximation accordingly. For each sample, three measurements were taken per run and repeated to obtain an average of six results.

3.3.3. Scanning Electron Microscopy (SEM)

Scanning (or sometimes known as secondary) electron microscopy (SEM) scans high energy electrons (excited by thermionic or electric field emission) across the surface of the substrate in a raster pattern under high vacuum. Lower energy, secondary electrons emitted off the surface are collected; the intensity of the output electrons depend on the angle of incidence of the emitted beam relative to the surface and the detector. The image produced contains information such as surface topology, composition and fractional coverage.

Samples need to be electrically conductive or coated in a conductor to prevent the accumulation of electrons at the surface, known as the "charging" effect. BDD particles were initially coated on a metal piece in powder form secured with sticky carbon tape. However, SEM analysis revealed image artifacts caused by uneven coverage.

Samples grown on the HFCVD reactor were highly boron doped and were assumed to be semi-metallic. All SEM images were obtained with a JEOL JSM 5600LV instrument.

3.3.4. Resistance Test for Electrical Conductivity

Low resistance ohmic contacts were used to allow charge to flow easily through the bulk of the substrate without changing the semiconductor characteristics. The non-uniformly doped boron in diamond suggests inhomogeneous conductivity through the substrate. Ag was used to form an ohmic contact with Si because it has good adhesion and high conductivity. Fabrication of the contacts onto the BDD thin films was done by physical vapour deposition using an Edwards vacuum evaporator.

An Si mask was placed on top of the samples and the exposed squares were positioned in the corners of the substrate about 0.2 cm away from the edges. A ball of silver wire was loaded into the Tungsten wire basket. Tungsten was used because of its high melting point (3422 °C) and low vapour pressure at high temperatures (> 1650 °C). The process was done under vacuum at 2×10^{-5} Torr and 50 nm Ag was deposited onto the substrates.

After deposition, the substrates were post-treated with ozone to ensure oxygen termination at the diamond surface. This provided an insulating layer in order to electrically isolate the contact components. This was done by the flow of ozone gas across UV light using a UVO 42A-220 (Jetlight Co. Inc) ozone cleaner and the surface of the diamond became oxidised.

The deposition process was repeated on the opposite face of the substrate i.e. Si side in order to measure resistivity through the substrate as well across the diamond face (Figure 15.) Ozone treatment on the bottom side of the substrate was not necessary as Si contains a native oxide layer. Resistance was measured using a digital multimeter and an average of three repeat measurements was taken. A pure p-type (100) Si substrate was used as a control for this part of the experiment.

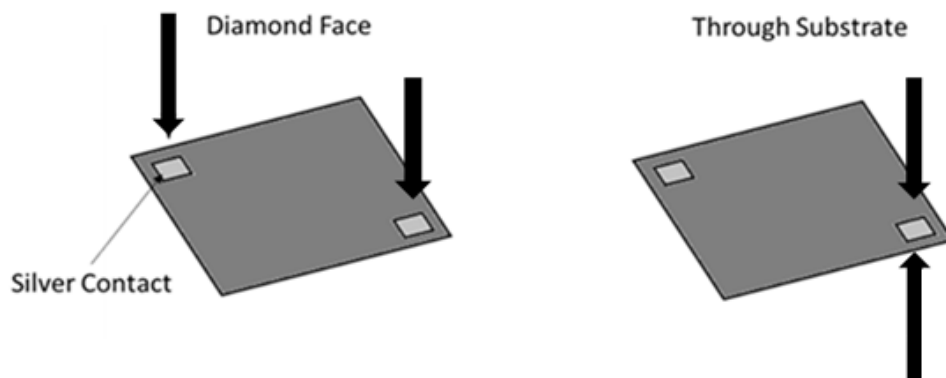


Figure 15. Two types of resistivity measurements were taken for each sample; arrows indicate position of the probes

4. Results and Discussion

4.1. pH Studies

Lowering the pH of PEI yielded a positive zeta potential (> 40 mV) but did not form favourable electrostatic interaction with the negatively charged diamond particles to form a stable suspension.

PEI contains charged NH groups which can be employed by adjusting pH. At lowered pH by addition of acetic acid, the polyelectrolyte protonates and has more positively charged surface groups. However, there is also an increased amount of CH_3COO^- counterions which increases the screening effect and also decreases the Debye length. Under neutral environments, i.e. in deionised water, the PEI solution is around pH 8-9 and is cationic. At a concentration of 5% it was able to form a stable suspension.

Under acidic conditions, PEI may become acid labile and subject to fragmentation. The viscosity of the solution decreases thus the stability of the suspension is reduced. The diamond surface may also become protonated. The attraction towards cationic groups is lost and hence the compatibility of the two components. This concludes that the suspension must be maintained at neutral to basic conditions in order to achieve stability.

4.2. DLS Measurements

Table 5. The average BDD particle diameter size in different media

Medium	Average Particle Size Diameter / d.nm	Standard Deviation / nm
Water	308	2.5
PEI 3 (0.1 wt%)	277	6
PEI 3 (5 wt%)	636	13
KOH / NaH_2PO_4 buffer	365	8

The results in (Table 5) show that centrifugation provides a narrower particle size distribution but does not eliminate the range of particle sizes. The particles range from around 150-650 nm and the average particle diameter size varies from solution to solution. The standard deviation appears to be larger with increase in average particle size; this is because larger particles have slower diffusion rates and are subject to gravitational effects. The count rate over multiple measurements was relatively unstable which indicated the reduction of particles lost due to sedimentation.

If the rate of sedimentation is lower than the rate of diffusion, the solution is said to be stable enough to take a successful DLS measurement. The above results fulfil this criterion but results with unstable count rates were discarded.

The average BDD particle diameter size is larger with polymer than with buffer. This may be due to the polymeric structure of PEI being dynamic in solution. If the adsorbed polymer later is lying flat against the surface of the particle, the apparent hydrodynamic size would be less than if the adsorbed polymer is dispersed out towards the medium. Regardless of which adsorbed state the polymer is in, the molecular weight is still be substantially higher than the solvated ions in the buffer solution, hence why the average particle size of BDD/PEI is nearly twice as large.

4.3. Zeta Potential Measurements

Table 6. Zeta potential values of BDD in various media and the values of each medium without the BDD particles

Sample	Medium	Zeta Potential/ mV	Standard Deviation / mV
BDD	Water	-18.4	3.07
PEI 1 (0.1 wt%)	Water	+2.42	0.0353
PEI 2 (0.1 wt%)	Water	+0.257	0.332
PEI 3 (0.1 wt%)	Water	+12.5	0.636
PEI 3 (0.2 wt%)	Water	+9.82	0.403
PEI 3 (5 wt%)	Water	+2.64	0.297
PEI 3 (0.1 wt%) pH6	10 wt% Acetic Acid	+41.4	2.05
BDD	PEI 3 (5 wt%)	+3.02	0.339
BDD	KOH/ NaH ₂ PO ₄ buffer	+19.05	0.200

Results in Table 6 show that apart from the zeta potential of the acidified PEI solution, none of the solutions were considered stable as the magnitude was less than 30 mV. The diamond particles suspended in water had a negative zeta potential which confirmed the terminating species to be negative (likely to be COO⁻). The mean coefficient of variation is calculated to be 16.7% which suggests precision is not high. Variation could be from the poor quality of the sample as the diamond particles were poorly suspended in de-ionised water.

Zeta potential decreases non-linearly with increase in concentration of PEI 3 (Figure 16) due to the increase in ionic strength. The number of counterions increase, polymer overlap concentration and hence the viscosity increases; the electrophoretic mobility decreases due to increased intermolecular interactions. This suggests that the diamond suspension should be prepared at minimal polyelectrolyte concentration in order to obtain maximal stability.

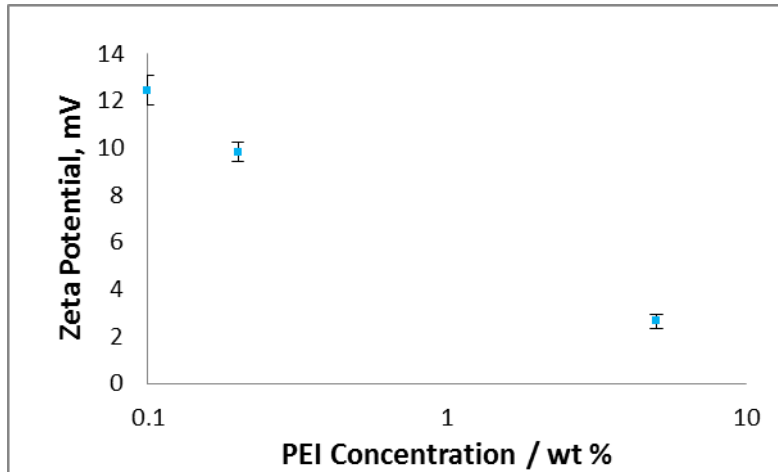


Figure 16. Zeta potential of PEI as a function of polymer concentration

However, the results for preparing the suspension show that the particles are visually most stable at the highest PEI concentration i.e. 5 wt%. This could be due to having a broad particle size distribution and failure to optimise concentration with size. Moreover, a higher concentration of PEI enhances the viscosity effects which slows down sedimentation and compensates for the loss in zeta potential.

Increasing the acidity of 0.1 wt% PEI 3 with 10 wt% acetic acid increases the zeta potential dramatically to > 40 mV but as discussed in 4.1, the suspension was not stable.

The zeta potential results for the relatively stable suspensions are both positive. This is unexpected as zeta potential should become more negative with increase in pH as the oxygen terminated diamond particles become deprotonated. The observation is interesting because the positive zeta potential may arise from the intrinsic properties of the starting material. The polycrystalline boron doped diamond is intrinsically a p-type material. Under the influence of an electric field, more electrons from the valence band are excited into the boron energy states, and thus the accumulation of holes may possibly generate a positive zeta potential.

In general, the bonding and configuration of boron in the nanodiamond lattice is not fully understood. It is not known whether boron sits within the grains or grain boundaries, and whether it is positioned within the bulk or the surface. Barnard et al. made predictions from theoretical studies showing that boron is likely to be situated at the grain boundary on the surface of isolated particles.⁴⁶

Similar results from Tsigkourakos's group reported the electrical probing of BDD seeds embedded into the interfacial layer of conductive diamond films.⁴⁷ In their report, the quoted zeta potential of BDD in water suspension was +21 mV which was also relatively unstable and resulted in low nucleation density.

The samples were slightly cloudy and of suitable refractive index for analysis. However, one systematic error could arise from the re-using of the disposable quartz capillary cells; the cells were flushed with deionised water and reused for the consecutive measurements. This may increase contamination and uncertainty of sample quality and the cells may also become damaged after prolonged use.

4.4. SEM Results

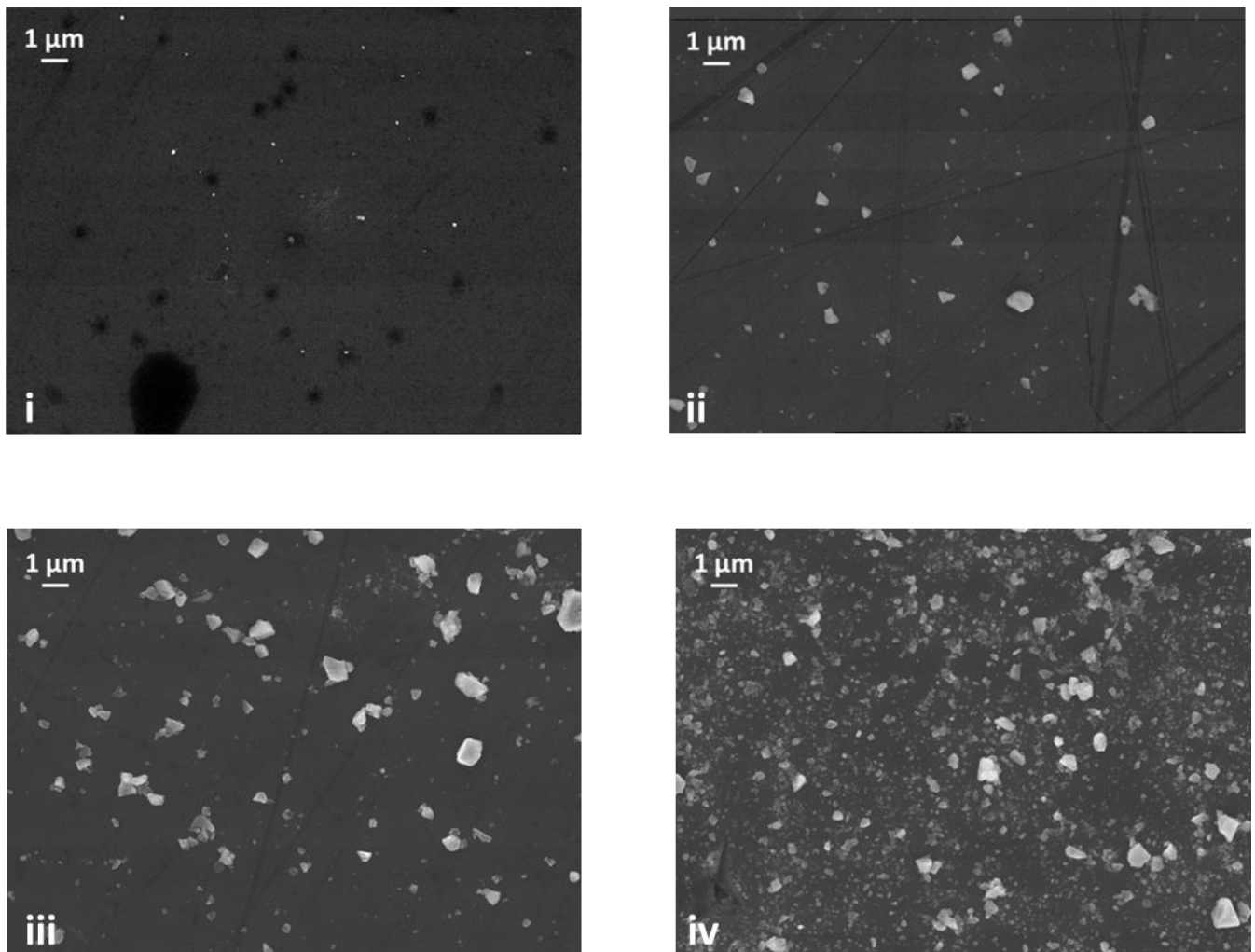


Figure 17. SEM micrographs showing the quality of seeded substrates using different techniques and seeds i.) substrate A, ii.) substrate C1, iii.) substrate C3 and iv.) substrate B1. All micrographs were taken prior to CVD growth. The dark marks are surface artefacts on the Si wafer

SEM micrographs were taken for substrates seeded with BDD nanoparticles prior to growth. This was done in order to assess the quality of the self-assembled substrates and to investigate whether the results were in agreement with DLS/ Zeta potential measurements.

Results in Figure 17 show substrate A has significantly low coverage compared to all other seeding methods used which suggests that a buffer may be a mediator for self-assembly. The low zeta potential value of +3.02 mV is a factor of low nucleation as the electrostatic attraction is low. Under CVD conditions, the SiC layer formed initially is slow due to the sparse layer of seeds. The resulting coalesced layer is relatively thick and this may have an impact on interfacial resistance. The lack of boron incorporation during the initial nucleation growth further suggests that substrate A is a poor candidate for attempts to enhance conductivity at the diamond/substrate interface.

Evaluation of substrates C1 and C3 show some improvements on coverage with longer self-assembly times. However, this may be an additive effect as opposed to self-assembly as substrate C3 was re-submerged into the BDD/buffer suspension a couple of times. In order to confirm which mechanism resulted in the coverage, the substrate should instead be exposed to the suspension for a longer period of time without disturbance.

Substrate B1 shows best coverage among all the other substrates that were pre-treated using a different seeding method. This could suggest that a combination of PEI and buffer promoted self-assembly via electrostatic attraction. However, substrates B and C are not directly comparable because the diamond concentration on the BDD/buffer solutions were different (C substrates were seeded with a more diluted suspension in order to achieve suspension stability). For this reason, a good coverage may predominantly result from sedimentation of a larger density of particles rather than self-assembled structures.

The zeta potential of the BDD/buffer solution was +19.05 mV, suggesting that PEI does not provide the adhesive layer that the polymer was designed to give during initial stages. The SEM micrographs are not in agreement with the zeta potential findings in this case, but as discussed previously, the enhanced seeding may be due to diamond concentration effects, and thus the results are not mutually exclusive.

Furthermore, PEI could possibly be providing an adhesive layer in a non-electrostatic sense. Due to the solution being naturally higher in viscosity than water, PEI could act as a high molecular weight “glue” that adheres long enough for the diamond particles to remain “stuck” to the surface. Thus the role of

PEI in enhancing nucleation is still in question, and its effects on interfacial resistance will be further discussed in section 4.5.

The SEM micrographs show a broad range of particle sizes as seen in DLS measurements. Attempts to measure particle size distribution and calculate nucleation density from the micrographs were carried out using ImageJ software. Particle diameter size was calculated assuming the particles were spheres for simplicity. The nucleation density was calculated by dividing the number of particles by the area of the each micrograph (scaled) and averaging the results of the all the micrographs taken per substrate sample. Results are shown in Table 7.

Table 7. Calculated nucleation density from SEM micrographs

Substrate	Calculated nucleation density / cm ⁻²
A	4.59×10^6
C1	2.02×10^7
C3	1.13×10^8
B1	6.70×10^8

As can be observed, the nucleation density of all the substrates is much lower than expected from seeding techniques, which typically yield around 10^{11} - 10^{12} cm⁻². A recent publication by Tsigkourakos et al. describes a similar seeding technique using a BDD in water suspension to seed (100) oriented Si substrates. They obtained a layer density of less than 10^9 cm⁻² which is also a relatively low value in comparison to seeding with undoped DND.⁴⁷ This may be due to the low zeta potential values of the BDD suspensions leading to the aggregation of BDD nanoparticles, and as a result there is less electrostatic attraction with the Si surface. Furthermore, the aggregation of particles could also lead to flocculation which explains why sedimentation appears to dominate over self-assembly.

As discussed previously, the seeding of the substrates may be an additive effect. The SEM micrographs show that prolonged exposure time of substrate in suspension appears to improve nucleation density. This is further confirmed by the calculated nucleation densities in Table 7. B substrates had the highest nucleation density of 6.70×10^8 cm⁻², indicating that the combination of polymer and buffer obtained the highest yield.

What is interesting is when the particle size distribution for each substrate was plotted (Figure 18), it can be seen that particles of < 150 nm were present on the substrate. This is not seen in DLS measurements despite the instrument's detection limits of 0.3 nm. One possible reason why it may be is because the

the dynamic light scattering technique measures the hydrodynamic radius of the diamond particles. Any changes to the surface of the particles changes the speed of diffusion and hence the apparent size of the particles. As explained in section 4.2, the polymeric structure of PEI is dynamic and the adsorbed state on the surface greatly affects the diffusion rate. The solvated ions in the BDD/buffer system could also alter the ionic concentration and change the apparent size.

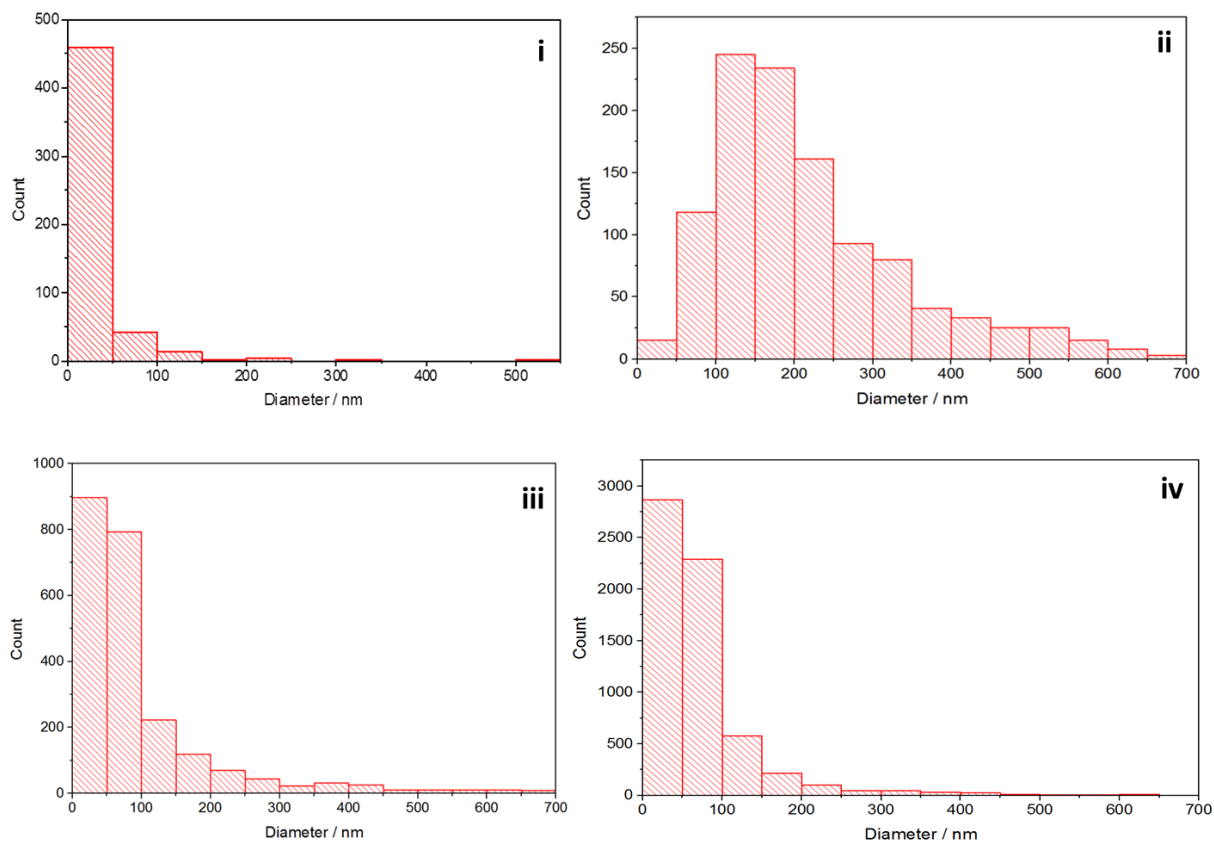


Figure 18. Particle size distribution calculated from SEM i.) substrate A, ii.) substrate C1, iii.) substrate C3 and iv.) substrate B1

In Figure 18, it could be seen that the majority of the particles are < 200 nm with the largest particles being < 700 nm. Substrate A has the lowest count in particles with the majority being ≤ 50 nm. It could be shown that in the presence of polymer only (i.e. without buffer), the particles that are successfully seeded onto the substrate are those that are not washed away due to viscosity effects.

It could be seen that there is a larger count and hence a higher nucleation density for substrate C3 compared with substrate C1 (plots labelled C and B respectively). Unusually, substrate C1 has a larger average particle diameter size than C3, suggesting that smaller particles begin to deposit onto the

substrate at a later stage of submersion. This demonstrates that although the seeding mechanism is initially dominated by gravitational effects, seeding in a self-assembled manner becomes more apparent over a longer period of time. This result is undesirable if the seeding technique aims to achieve a uniformly dispersed monolayer of nanoparticles that is less than a few nm thick. Improvements on zeta potential of the BDD suspension is necessary for the seeding mechanism to be in favour of electrostatic attraction.

Substrate B1 (plot labelled D) has the largest count and the majority of particles are ≤ 50 nm. This implies that a combination of polymer and buffer enhances all the effects described above (viscosity, particle size and electronic stabilisation). Despite this, there is still a need for further optimisation of the seeding technique in order to gain an increased fractional coverage and a narrower particle size distribution.

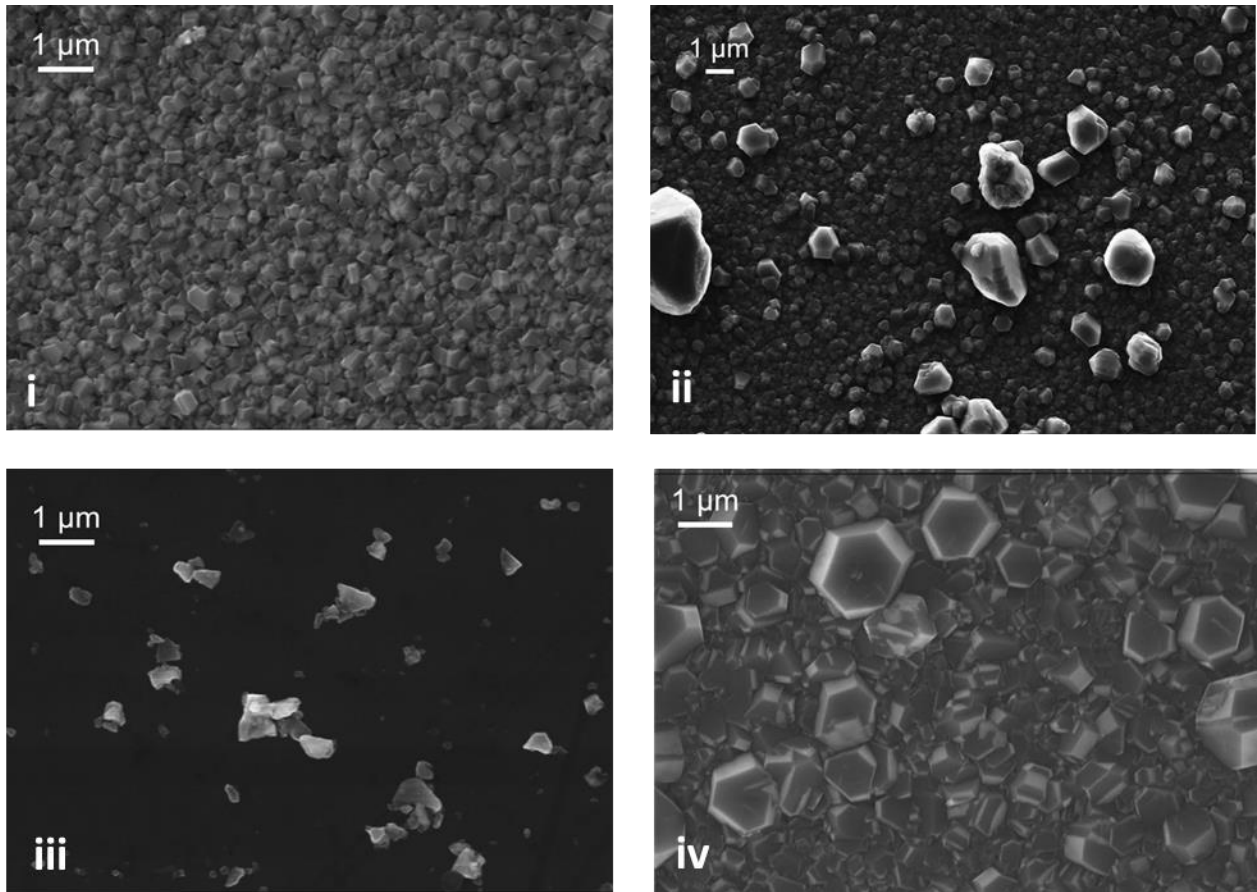


Figure 19. SEM micrographs of i.) BDD grown on substrate D1 for 1 hour at 1.24% B_2H_6/CH_4 and 1% CH_4/H_2 concentration, ii.) BDD grown on substrate B3 for 30 minutes at 1.24% B_2H_6/CH_4 and 1% CH_4/H_2 concentration, iii.) substrate B1 prior to CVD growth, and iv.) BDD grown on substrate B1 for 1 hour at 1.24% B_2H_6/CH_4 and 1% CH_4/H_2 concentration.

Figure 19 compares the surface morphology of doped seeds with undoped after CVD growth. The SEM micrographs show the morphology of faceted nano- to micro-crystalline diamond layers after CVD growth; the grain size of the films are largely determined by the CVD conditions and specifically the ratio of methane to hydrogen gas. An increase in the ratio of methane from 1 % to 5 % CH₄/H₂ decreases the grain size and eventually forms nanocrystalline structures that appear smoother, non-faceted and more “cauliflower” shaped.⁴⁸ After 1 hour growth at 1 % CH₄/H₂, the grain sizes in substrates D1 and B1 are in the nano- to microscale region, but the grain boundaries and shapes of the crystals greatly resemble that of microcrystalline diamond. It is predicted that microcrystalline diamond will eventually form at prolonged growth using this concentration of methane.

The facets grown from doped seeds are much rougher and inhomogeneous compared with facets grown from DND. This is because the parent BDD seeds are pulverised into a variety of sizes and shapes thus directs columnar growth in a more randomised manner; this also results in larger grain sizes (~ 0.5-1 µm) compared with using undoped seeds (~ 100-500 nm). Addition of B₂H₆ during CVD shows that B is incorporated into both the (100) and (111) lattice planes, with several studies showing preferential growth on the (111) faces.⁴⁹ The growth parameter α is defined as the ratio of (100) to (111), where v_{100} and v_{111} are growth velocities of the respective lattice planes.

$$\alpha = \sqrt{3} \frac{v_{100}}{v_{111}}$$

Equation 2. Growth parameter derived from homoepitaxial data⁵⁰

Empirically, the growth parameter depends on the methane concentration, the substrate temperature and the impurity gases present. Laser interferometry studies show that nitrogen was found to increase the growth rate on (100), thereby increasing α , whereas boron increases the growth rate on (111) thus decreases α .⁵¹ Unusually, from looking at substrate B3 (SEM micrograph labelled C in Figure 19), the deposition rate appears to be fast, and a continuous film was formed after just 30 minutes growth time.

The boron incorporation can occur via a ring opening mechanism as in the case of carbon incorporation, or by direct insertion in the C-C bond on the diamond (100) surface. BH_x species can be lost via hydrogen abstraction to form boron containing gas species which diffuse away from the surface. Computational studies show that both B incorporation and B loss processes are energetically less demanding than the corresponding carbon processes.⁴⁹ This suggests that a low α infers decreased undoped growth but does not account for the possibility of enhanced BDD growth.

There is a possibility that PEI may be decomposed to CO₂/CO/nitrous oxides during the stage heating step prior to CVD growth. When nitrogen containing compounds (as in the case of PEI) are exposed to high growth temperatures, the nitrogen can diffuse through the lattice and enhance v_{100} hence the growth factor. Indeed, recent studies show that the use of nitrogen during boron doping has been found to improve surface morphology and growth rate of BDD films.⁵²

Looking at the SEM micrographs more closely, the morphology of substrate D1 (labelled A in Figure 19) comprises of triangular twinned (111) facets and cubic (100) crystal facets, a characteristic of BDD material. Surprisingly, the BDD grown on substrate B1 (labelled D) shows a more dominant growth on (111) planes and the resulting morphology is a series of truncated tetrahedron, twinned plates and octahedral morphologies. The difference may arise from the increased boron concentration derived from the parent seeds which induces this preferential growth.

4.5. Resistance Measurements

Table 8. Resistance values across the surface of the substrate and through the substrate

Substrate	CVD Conditions	Diamond Face / Ω	Standard Deviation / Ω	Through the Substrate / Ω	Standard Deviation / Ω
B1	High [B], 1 hour	29.62	0.21	543.33	57.73
B2	Low [B], 1hour	125.33	1.15	1160.00	17.32
B3	High [B], 30 minutes	147.67	0.58	1523.33	118.46
C3	High [B], 1 hour	42.67	0.58	21.63	0.06
D1	High [B], 1 hour	95.33	0.21	41.00	1.00
D2	Low [B], 1 hour	146.00	23.27	30.90	0.17
D3	High [B], 30 minutes	180.26	0.46	118.33	14.43
Si wafer	-	2323.33	73.71	24825.00	5012.24

In general, as seen from Table 8, the substrates with lower boron incorporation during CVD growth have higher resistance than substrates with higher boron content. This is an intrinsic property of doping, as higher levels of doping lead to increased conductivity as more electrons are promoted to the empty acceptor levels. The difference in resistance varies from about 1.5 to 4 times more resistant with low boron content materials. The reproducibility is mostly high as seen from the calculated standard errors, but the values are not representative of the true resistance of the material, as seen from the varied results and sparse trends.

There could be several factors that could affect the resistance of the material. This includes the thickness of the material after CVD growth, the quality of the seeding (seed size, nucleation

density...etc.) and the quality of the surface post treatment (ozone treatment). UV/Ozone treatment does not guarantee uniform functionalization of surfaces. Optimisation of the treatment time largely depends on the nature and the condition of the substrate prior to treatment. 30 minutes exposure time may not have provided complete oxygen coverage and some reports describe treatment times of ≥ 60 minutes.^{53,54}

The resistance measurements through the substrate show that the B substrates were significantly more resistant than the C and D samples. This may be because the set decomposition time for PEI was not long enough and that a resistive polymeric layer may be absorbed. Although PEI is charged upon solvation, it is unlikely this facilitates current flow as the dry polymer is uncharged and mostly made up of its long carbon backbone. Also, PEI is a nitrogen containing compound and as mentioned in section 4.4, there have been reports highlighting that nitrogen provides a feedstock for undoped diamond growth under CVD conditions. The enhanced undoped diamond deposition may in effect increase the resistance of the resulting diamond film.

Comparing the C substrate with D, that is BDD in buffer solution and DND as seeds respectively, the resistance values were only marginally different, with the doped seeds being slightly less resistant. One possible reason could be due to the set CVD conditions that were chosen. Under high growth temperatures, there could be a chance of B_2H_6 gas diffusing into the undoped seeded layer and substitute the carbon atoms with boron. However, it has been reported that thermal diffusion gives relatively low B incorporation of about 3×10^{19} atoms cm^{-2} at a shallow depth of 500 Å, and thus may not fully account for the observed resistance values in substrates C and D.⁵⁵

After the bead milling process, the BDD nanoparticles are expected to be as conductive as the parent CVD grown film. Milling is a physical process and thus applying mechanical stress should not modify its chemical structure, thus its electrical conductive pathways should remain the same. However, due to non-uniformity of the size of the seeds, the seeded layer has a more pronounced roughness and larger grain boundaries, resulting in poorer coalescence during CVD growth. On the other hand, the undoped seeds are all the same size (36 nm) and thus the resulting seeded films are more homogeneous, less thick and have smaller grain sizes.

5. Conclusion

Boron doped diamond (BDD) is an excellent material for semiconductor applications and electrochemical analysis. This material can be synthesised using CVD. Seeding of the substrate is required to initiate CVD growth during the induction period. Conventional methods of seeding non-diamond substrates include using detonation nanodiamond particles (DND) as seeds, or depositing diamond powder via the abrasion technique. However, these methods use undoped diamond particles; as a result this forms an insulating barrier at the diamond-substrate interface. This is highly unfavourable for applications that involve the flow of current through the diamond material and substrate.

There has been a recent emergence of using boron doped nanodiamond particles as seeds for non-diamond substrates. This novel seeding technique describes the elimination of the insulating layer that originates from undoped seeds. Boron incorporation via ion implantation is a destructive method, and CVD growth is impractical without the initial induction period of nucleated seeds. The project describes efforts to show that interfacial resistance is reduced upon incorporation of BDD seeds.

BDD nanoparticles were created by pulverising a microcrystalline as-purchased BDD CVD diamond in the bead milling machine for 7 hours. The resulting crushed film was used to create a stable diamond suspension, which was subsequently seeded onto non-diamond (001) p-type Si substrates via self-assembly.

Several seeding methods were attempted and the quality and nucleation density was evaluated using SEM. DLS measurements show a large particle size distribution and that the solvated particles were around 150-650 nm in hydrodynamic diameter. However, the particle sizes calculated from SEM images were not in agreement with DLS results, revealing the majority of the particles were around 100 nm in diameter. The difference is from the hydration of particles in the suspension used in DLS and thus particle size calculated from SEM may be more representative of the diamond particles.

It was shown the best seeded substrate resulted from the method that uses a combination of cationic polymer PEI and an alkaline buffer, and these substrates were labelled as "B substrates" in this report. The B substrates were consequently selected and grown under CVD conditions; the surface morphology and growth rates were interpreted. Comparison with undoped equivalents (D substrates) was also made using DND as the undoped candidate.

Both types of substrates revealed (111) and (100) crystal facets which is a dominant characteristic of boron doped diamond. B substrates contained a larger amount of (111) twinned material perhaps due to the intrinsic abundance found in the parent BDD seeds. Moreover, the seeded layer comprised of a variety of seed sizes; hence the resulting grown BDD was rougher and contained larger grain sizes.

A continuous film had already formed within 30 minutes of CVD growth; the growth rate is higher than expected as it is known boron increases v_{111} hence decreases the growth parameter α . It is suspected that nitrogen was present during CVD growth. The N source may derive from the PEI which had not been completely decomposed prior to CVD growth, or had diffused into the reactor during the stage heating process. This may be a reason for the fast growth rate as nitrogen is known to enhance v_{100} and hence the growth parameter.

Resistance measurements were inconclusive of which seeding technique provided the best conductivity enhancement at the diamond-substrate interface. It also failed to show that doped seeds reduced the interfacial resistance in comparison with undoped seeds. This may be a cause of several factors, such as the incomplete surface functionalization in the ozone treatment process, the inconsistency of particle sizes used for doped seeding, and nitrogen from the PEI enhancing undoped diamond growth.

6. Future Work

6.1. Method Development

6.1.1. DLS - Method Development

In order to gain more confidence in the DLS data, measurements should be repeated for a wider range of concentrations over a wider range of pH. If the sample concentration was too low, the level of scattered light may be too low and the data becomes noisier. The sample also becomes more sensitive to impurities and this was seen in some samples where anomalous particle sizes were detected.

If the sample concentration was too high, the particles may interact with one another and diffusion may be restricted. The particle size may no longer be independent of concentration; size results become distorted and aggregate formation could be seen. The number of back-scattered photons also increases as more particles are present, leading to multiple scattering.

6.1.2. Zeta Potential Measurements – Method Development

Improvements on zeta potential of the BDD suspension is necessary for the seeding mechanism to be in favour of electrostatic attraction as opposed to gravitational effects. A wider variety of polymers and solvents such as poly(diallyldimethylammonium chloride) (PDDA) or methanol could be tested. In order to reduce aggregation caused by low zeta potential values and unstable suspensions, the sonication time could be increased to ensure a more dispersed solution. The zeta potential should also be measured over a wider pH range and concentrations as mentioned previously.

6.1.3. Resistance Measurements - Method Development

As seen from SEM and DLS analysis, there is a broad particle size distribution in the bead milled BDD nanoparticles even after centrifugation processes. In contrast, the undoped seeds originated from an ultradispersed DND solution, with a uniform diameter size of 36 nm. Evidently, the size and uniformity of the two samples are incomparable, and hence the diagnosis of their difference in interfacial resistance is somewhat trivial.

A more uniformly seeded layer can provide a more nucleated surface, resulting in thinner films and better connected electronic pathways. In order to interpret the two samples more meaningfully, the BDD nanoparticles must achieve a smaller and more uniform size. This may be achieved by increasing the time of bead milling and improving the size separation process. On the other hand, perhaps a more

facile approach is to increase the size of the undoped seeds perhaps via short exposure time in the CVD reactor.

There has been a recent publication in an established model linking the size of the seeds and nucleation density to the interfacial resistance; the model agrees well with their experimental findings. The contribution of undoped seeds to increased interfacial resistance is suggested to be insignificant if the undoped density is less than $5 \times 10^{10} \text{ cm}^{-2}$ for particles of 20 nm in diameter size.⁵⁶

6.2. Further Suggestions

In order to confirm whether nitrogen was present during chemical vapour deposition, substrates that were grown with BDD nanoparticles in the absence of PEI should be screened. SEM characterisation should reveal the difference in crystal morphologies and growth rates.

The amount of diamond and non-diamond content can be characterised using Raman spectroscopy by obtaining the $sp^2:sp^3$ carbon ratio. Raman data have not been included in this report because the background noise was too high and the graphite/diamond peaks could not be identified. This is because the area of the diamond peak decreases with increasing boron dopant levels. One possible explanation is the interference caused by the charged hole carriers which interact with the optic phonons from the laser. Longer acquisition times are therefore necessary in order to increase the frequency count hence gain better signal.

Scanning ion mass spectroscopy is a powerful analytical technique which identifies the different layers of the material (in this case the diamond film, the seeded layer and the silicon substrate). In other words, this technique shows whether there is a difference in the position and concentration of dopant atoms found in the seeded layer and the grown layer. Observing a difference implies a decay in conductivity as it approaches the substrate, hence provides an indicator of the quality of the BDD seeded layer. Other techniques that could provide useful information include TEM or AFM to study the orientation of the boron atoms within the crystal lattice.

In order to investigate more ways to study the resistance of the materials, the diamond interfacial layer can be electrically probed with nanoscale resolution using scanning spreading resistance microscopy (SSRM). This is a scanning probe microscopy which in essence is similar to AFM, and is a well established technique for characterising nanoscale semiconductor device structures.⁴⁷

-
- ¹ P. May, *Philos. Trans. R. Soc. London.*, 2000, **358**, 473-495
- ² J.E. Field, *Cryst. Res. Technol.*, 1992, **28**, 602
- ³ M.H. Nazare, A.J. Neves, *Properties, Growth and Applications of Diamond*, INSPEC, London, 2001
- ⁴ M.N.R. Ashfold, P.W. May, C.A. Rego, N.M. Everitt, *Chem. Soc. Rev.*, 1994, **23**, 21-30
- ⁵ H. Nakayama, H. Katayama-Yoshida, *J. Phys.: Condens. Matter*, 2003, **15**, 1077-1091
- ⁶ J.J. Gracio, Q.H. Fan, J.C. Madaleno, *J. Phys. D: Appl. Phys.*, 2010, **43**, 374017
- ⁷ J.P. Mercier, G. Zambelli, V. Kurz, *Introduction to Materials Science*, Elsevier, France, 2002, 349
- ⁸ R.J.D. Tilly, *Understanding Solids: The Science of Materials*, John Wiley and Sons, England, 2013
- ⁹ L. Diederich, O.M. Kuttel, P. Ruffieux, T. Pillo, P. Aebi, L. Schlapbach, *Surf. Sci.*, 1998, **417** (1), 41-52
- ¹⁰ H. Kato, T. Makino, S. Yamasaki, H. Okushi, *J. Phys. D: Appl. Phys.*, 2007, **40**, 6189
- ¹¹ L.S. Pan, D.R. Kania, *Diamond: Electronic Properties and Applications*, Springer, England, 1995
- ¹² P.M. Quaino, W. Schmickler, *ChemElectroChem*, 2014, **1** (5), 933-939
- ¹³ N. Yang, *Novel Aspects of Diamond: From Growth to Application*, Springer, Switzerland, 2015, 9
- ¹⁴ R. Kalish, *J. Phys. D: Appl. Phys.*, 2007, **40**, 6467
- ¹⁵ T. Yamada, M. Hasegawa, Y. Kudo, T. Mazusawa, *Vacuum Nanoelectronics Conference (IVNC), 2011 24th International*, Wuppertal, IEEE, 2011, 125-126
- ¹⁶ K.E. Bennet, K.H. Lee, J.N. Kruchowski, S-Y. Chang, M.P. Marsh, A.A.V. Orsow, A. Paez, F.S. Manciu, *Materials*, 2013, **6**, 5726- 5741
- ¹⁷ E. A. Ekimov , V.A. Sidorov , E.D. Bauer , N.N. Mel'nik , N.J. Curro , J.D. Thompson, S.M. Stishov, *Nature*, 2004, **428**, 542-545
- ¹⁸ Y. Takano, M. Nagao , K. Kobayashi , H. Umezawa , I. Sakaguchi , M. Tachiki , T. Hatano , H. Kawarada, *Appl. Phys. Lett.*, 2004, **85**, 2851
- ¹⁹ J.E. Field, *The Properties of Diamond*, Academic Press, New York, 1979
- ²⁰ P. May, *Endeavour*, 1995, **19**(3), 101-106
- ²¹ M. Ashfold, P. May, *Chem. Ind.*, 1997, **13**, 505-508
- ²² P.K. Bachmann, D. Leers, H. Lydtin, *Diamond Relat. Mater*, 1991, **1**, 1
- ²³ H. Liu, D.S. Dandy, *Diamond Relat. Mater*, 1995, **4**, 1173
- ²⁴ S.T. Lee, Z. Lin, X. Jiang, *Mater. Sci. Eng., R*, 1999, **25**, 123
- ²⁵ X. Jiang, K. Schiffman, C.P. Klages, *Phys., Rev., B*, 1994, **50**, 8402-8410
- ²⁶ S. Yugo, T. Kanai, T. Kimura, T. Muto, *Appl. Phys. Lett.*, 1991, **58** (10), 1036-1038
- ²⁷ J.C. Arnault, S. Saada, S. Delclos, L. Rocha, L. Intiso, R. Polini, A. Hoffmann, S. Michaelson, P. Bergonzo, *Chem. Vap. Deposition*, 2008, **14**, (7-8), 187-195
- ²⁸ K.B. Holt, *Philos. Trans. R. Soc., A.*, 2007, **365**, 2845-2861
- ²⁹ S. Heyer, W. Janssen, S. Turner, Y.G. Lu, W.S. Yeap, J. Verbeeck, K. Haenen, A. Krueger, *ACS Nano*, 2014, **8** (6), 5757-5764
- ³⁰ R. Willardson, E.R. Weber, C. Christofides, G. Ghibaudo, *Effect of Disorder and Defects in Ion-Implanted Semiconductors: Electrical and Physiochemical Characterization, Volume 45 (Semiconductors & Semimetals)*, Academic Press, San Diego, 1997
- ³¹ W. Janssen, Doctoral Dissertation, Hasselt University, 2014
- ³² Y. Liang, M. Ozawa, A. Kruger, *ACS Nano*, 2009, **3** (8), 2298-2296
- ³³ J. Cheng, J. He, C. Li, Y. Yang, *Chem. Mater.*, 2008, **20**, 4224
- ³⁴ L. Pastewka *et al*, *Nature Mater.*, 2011, **10**, 34-38
- ³⁵ O. Williams, J. Hees, C. Dieker, W. Jager, L. Kirste, C. Nebel, *ACS Nano*, 2010, **4** (8), 4824-4830
- ³⁶ I. Zhitomirsky, *Mater. Lett.*, 1998, **37**, 72-78
- ³⁷ A.M. Panich, A.E. Aleksenskii, *Diamond Relat. Mater.*, 2012, **27-28**, 45
- ³⁸ M. Ozawa, M. Inakuma, M. Takahashi, F. Kataoka, A. Krueger, E. Osawa, *Adv. Mater.*, 2007, **19**, 1201
- ³⁹ O.A. Williams, *Nanodiamond*, RSC, Cambridge, 2014
- ⁴⁰ M. Yoshimura, K. Honda, T. Kondo, R. Uchikado, Y. Einagra, T.N. Rao, D.A. Tryk, A. Fujishima, *Diamond Relat. Mater.*, 2002, **11**, 67-74
- ⁴¹ L.A. Hutton, J. G. Iacobini, E. Bitziou, R.B. Channon, M. E. Newton, J.V. Machpherson, *Anal. Chem.*, 2013, **85** (15), 7230-7240

-
- ⁴² F.A.M. Koeck, R.J. Nermanek, J. Sharp, *Vacuum Nanoelectronics Conference (IVNC), 2013 26th International*, Roanoke, Virginia, IEEE, 2013, 1-3
- ⁴³ K.M. O'Donnell, T.L. Martin, N.A. Fox, D. Cherns, *Mater. Res. Soc. Symp. Proc.*, 2011, **1282**, 163-168
- ⁴⁴ A. J. Neves, M.H. Nazare, *Properties, Growth and Applications of Diamond*, INSPEC, London, 2001, 73-74
- ⁴⁵ *US Pat.*, 20100233371, 2009
- ⁴⁶ A.S. Barnard, M. Sternberg, *J. Phys. Chem. B.*, 2006, **110**, 19307-19314
- ⁴⁷ M. Tsigkourakos, T. Hantschel, C. Bangerter, W. Vandervorst, *Phys.Status Solidi.A*, 2014, **211** (10), 2284-2289
- ⁴⁸ P. May, M. Ashfold, *J. Appl. Phys.*, 2007, **101** (053115), 1-9
- ⁴⁹ A. Cheesman, J. Harvey, M. Ashfold, *Phys. Chem. Chem. Phys.*, 2005, **7**, 1121-1126
- ⁵⁰ S. Koizumi, C. Nebel, M. Nesladek, *Physics and Application of CVD Diamond*, Wiley-VCH, Weinheim, 2008, 36
- ⁵¹ M. Werner, R. Locher, *Rep. Prog. Phys.*, 1998, **61**, 1665-1710
- ⁵² S.K. Karna, Y.K. Vohra, P. Kung, S.T. Weir, *J. Mater. Sci.* 2014, **3**, 43-49
- ⁵³ K.S. Song, T. Sakai, H. Kanazawa, Y. Araki, H. Umezawa, M. Tachiki, H. Kawarado, *Biosens. Bioelectron.* 2003, **19**, 137-140
- ⁵⁴ V. Seshan, D. Ullien, A. Castellanos-Gomez, S. Sachdeva, D.H.K. Murthy, T.J. Savenjie, H.A. Ahmad, T.S. Nunnay et al, *J. Chem. Phys.*, 2013, **138**, 234707
- ⁵⁵ W. Tsai, M. Delfino, D. Hodul, M. Riazat, L.Y. Ching, G. Reynolds, C.B. Cooper, *IEEE*, 1991, **12** (4), 157-159
- ⁵⁶ M. Tsigkourakos, T. Hantschel, D.K. Simon, T. Nuytten, A.S. Verhulst, B. Douhard, W. Vandervorst, *Carbon*, 2014, **79**, 103-112